THE JOURNAL OF BIOLOGICAL CHEMISTRY VOL. 291, NO. 25, pp. 13175–13193, June 17, 2016

The Dynamics and Turnover of Tau Aggregates in Cultured Cells

INSIGHTS INTO THERAPIES FOR TAUOPATHIES[*S]

Received for publication, December 21, 2015, and in revised form, March 28, 2016 Published, JBC Papers in Press, April 18, 2016, DOI 10.1074/jbc.M115.712083

Jing L. Guo[‡1], Arjan Buist[§], Alberto Soares[§], Kathleen Callaerts[§], Sara Calafate[§], Frederik Stevenaert[§], Joshua P. Daniels[‡], Bryan E. Zoll[‡], Alex Crowe[‡], Kurt R. Brunden[‡], Diederik Moechars[§], and Virginia M. Y. Lee[‡2]

From the [‡]Department of Pathology and Laboratory Medicine, Institute on Aging and Center for Neurodegenerative Disease Research, University of Pennsylvania School of Medicine, Philadelphia, Pennsylvania 19104 and the [§]Neuroscience Department, Janssen Research and Development, a Division of Janssen Pharmaceutica NV, 2340 Beerse, Belgium

Filamentous tau aggregates, the hallmark lesions of Alzheimer disease (AD), play key roles in neurodegeneration. Activation of protein degradation systems has been proposed to be a potential strategy for removing pathological tau, but it remains unclear how effectively tau aggregates can be degraded by these systems. By applying our previously established cellular model system of AD-like tau aggregate induction using preformed tau fibrils, we demonstrate that tau aggregates induced in cells with regulated expression of full-length mutant tau can be gradually cleared when soluble tau expression is suppressed. This clearance is at least partially mediated by the autophagy-lysosome pathway, although both the ubiquitin-proteasome system and the autophagy-lysosome pathway are deficient in handling large tau aggregates. Importantly, residual tau aggregates left after the clearance phase leads to a rapid reinstatement of robust tau pathology once soluble tau expression is turned on again. Moreover, we succeeded in generating monoclonal cells persistently carrying tau aggregates without obvious cytotoxicity. Live imaging of GFP-tagged tau aggregates showed that tau inclusions are dynamic structures constantly undergoing "fission" and "fusion," which facilitate stable propagation of tau pathology in dividing cells. These findings provide a greater understanding of cell-to-cell transmission of tau aggregates in dividing cells and possibly neurons.

Filamentous aggregates made up of hyperphosphorylated tau protein are the defining pathological feature of numerous neurodegenerative diseases, such as Alzheimer disease, corticobasal degeneration, progressive supranuclear palsy, and Pick disease, which are collectively termed tauopathies (reviewed by Ref. 1). Physiologically, tau is a highly soluble microtubule-associated protein important for the assembly and stability of microtubules (2, 3). Insoluble, aggregated tau that is hyperphosphorylated and conformationally altered not only loses its physiological role of binding microtubules, but can also physically interfere with normal functioning of other cellular components (reviewed by Ref. 4). Strong correlations of the distribution and severity of tau pathology with clinical phenotypes of tauopathy patients (5–7) support the key contribution of aggregated tau to neuronal dysfunction and degeneration in these diseases, although some studies suggest pre-fibrillar tau species, such as oligomers, could be equally, if not more toxic than mature tau fibrils (8–11).

One obvious strategy to treat tauopathies is to remove intracellular tau aggregates either by promoting the disassembly of tau fibrils or by activating cellular degradation machineries to clear these toxic entities. A recent study demonstrated that it is possible to reverse mature tau inclusions together with associated neuronal deficits by suppressing soluble tau expression in a mouse model with inducible expression of tau, but the exact mechanism of tau pathology clearance was not explored (12). There are two primary protein degradation systems in cells, the ubiquitin-proteasome system (UPS),[3] which is responsible for the turnover of soluble and/or short-lived proteins, and the autophagy-lysosome pathway (ALP), which is important for the degradation of insoluble and/or longer-lived proteins as well as damaged cellular organelles (reviewed by Ref. 13). The majority of existing studies on tau degradation focused on soluble or monomeric tau, which was shown to be the substrate of both UPS and ALP (reviewed by Ref. 14). Several papers demonstrated that stimulation of autophagy by trehalose or rapamycin can ameliorate tau pathology both in cultured cells and transgenic mice overexpressing mutant tau (15–17). However, it is not clear whether autophagy participates in the basal degradation of insoluble tau without pharmacological activation. More importantly, tau aggregates induced purely by overexpression

* This work was supported, in whole or in part, by National Institutes of Health NIA Grant AG17586, the CurePSP Foundation, and a postdoctoral fellowship award (to J. L. G.) from Sophie M. Moyer and other donors of the Alzheimer's disease research program of the BrightFocus Foundation. Some coauthors work for Janssen, Pharmaceutical Companies of Johnson & Johnson. The content is solely the responsibility of the authors and does not necessarily represent the official views of the National Institutes of Health.

[S] This article contains supplemental Movies S1–S4.

[1] To whom correspondence may be addressed: Center for Neurodegenerative Disease Research, Dept. of Pathology and Laboratory Medicine, 3rd floor Maloney Bldg., 3600 Spruce St., Philadelphia, PA 19104-4283. Tel.: 215-662-6427; Fax: 215-349-5909; E-mail: guojing@mail.med.upenn.edu.

[2] To whom correspondence may be addressed: Center for Neurodegenerative Disease Research, Dept. of Pathology and Laboratory Medicine, 3rd floor Maloney Bldg., 3600 Spruce St., Philadelphia, PA 19104-4283. Tel.: 215-662-6427; Fax: 215-349-5909; E-mail: vmylee@upenn.edu.

[3] The abbreviations used are: UPS, ubiquitin-proteasome system; AD, Alzheimer disease; ALP, autophagy-lysosome pathway; α-Syn, α-synuclein; BafA1, bafilomycin A1; c-lac, clasto-lactacystin β-lactone; CQ, chloroquine diphosphate; Dox, doxycycline; epox, epoxomicin; PFA, paraformaldehyde; PFF, preformed fibril; ANOVA, analysis of variance.

of mutant tau in these models may be qualitatively different from authentic tau pathology developed in diseased brains (18, 19). Furthermore, whereas inhibition of ALP has been shown to induce tau deposition (20–22), the effect of tau aggregation on ALP has not been well studied.

We previously established a cell model with robust tau aggregates closely resembling neurofibrillary tangles in the AD brains, whereby preformed tau fibrils (tau PFFs) were transduced into QBI-293 cells transiently transfected with mutant tau to "seed" the fibrillization of soluble tau (18). We now adapt this model to a stable cell line with inducible expression of mutant tau, which allows us to study the turnover of tau aggregates upon suppression of tau expression. A GFP tag attached to the overexpressed tau further enables us to directly visualize the dynamics of PFF-induced tau aggregates through live imaging. In addition, we successfully generated a clone stably carrying tau aggregates due to faithful propagation of misfolded tau seeds to daughter cells during cell division. With the improved system, we found that tau aggregates can be gradually cleared from cells when soluble tau expression is turned off and this clearance process is at least partially mediated by the ALP. However, the presence of even a minute amount of residual aggregates is sufficient to rapidly reinstate tau aggregation once tau expression is turned on again. These observations increase our understanding of cellular responses to tau aggregates, and have implications regarding therapeutic strategies directed toward modulation of tau expression or enhancement of the ALP pathway in tauopathies.

Experimental Procedures

Cell Culture and Generation of Stable Cell Lines with Inducible Expression of Tau—Human embryonic kidney-derived QBI-293 cells (QBiogene) were grown in Dulbecco's modified Eagle's medium supplemented with 10% heat-inactivated fetal bovine serum (FBS), 1% pyruvate (10 mM), 1% penicillin-streptomycin and L-glutamine (20 mM). Cells were maintained at 37 °C in humidified atmosphere containing 5% CO_2.

To generate stable cell lines expressing full-length human tau T40 (2N4R) carrying the P301L mutation with a GFP tag (T40/P301L-GFP), 1 day prior to transfection, 80% confluent QBI-293 cells were trypsinized and then plated at 1.5×10^6 in a 10-cm dish. The growth medium was renewed directly before transfection. DNA mixture containing 2.5 μg of pcDNA6-TR and 2.5 μg of pcDNA4/TO-T40/P301L-GFP was diluted in 500 μl of Opti-MEM (Invitrogen) and 15 μl of FuGENE® 6 Transfection Reagent (Roche Applied Science) diluted in 500 μl of Opti-MEM was added. The mixture was incubated for 15 min at room temperature and then added to the cells. After 24 h incubation, the growth medium was removed and replaced with fresh medium containing 5 μg/ml of blasticidin and 200 μg/ml of Zeozin. Monoclonal lines were generated by limited dilution of drug-resistant cells and thereafter grown in full medium containing tetracycline-screened FBS and the same concentrations of selection drugs. Clone 4 stably expressing T40/P301L-GFP was selected for use in this study.

Tau PFF Generation and Transduction—The cDNA coding for Myc-K18 containing the P301L mutation (Myc-K18/P301L) was cloned into pRK172 bacterial expression vector. After expression in BL21(DE3) RIL cells, recombinant Myc-K18/P301L was purified by cationic exchange using a fast protein liquid chromatography (FPLC) column as described previously (23). Preformed Myc-K18/P301L fibrils (tau PFFs) were generated by mixing 40 μM purified recombinant Myc-K18/P301L with 40 μM low molecular weight heparin and 2 mM DTT in 100 mM sodium acetate buffer (pH 7.0) and incubated at 37 °C for 3 days without agitation. Prior to being used on cells, the fibrillization mixture was centrifuged at 100,000 $\times$ *g* for 30 min at 22 °C and the resulting pellet was re-suspended in equal volume of 100 mM sodium acetate buffer (pH 7.0) without heparin and DTT.

Tau PFF transduction was performed using BioPORTER reagent as previously described (18). Briefly, 80 μl of 10 μM sonicated Myc-K18/P301L fibrils were added to one tube of BioPORTER reagent. After gentle mixing and 10 min incubation at room temperature, the fibril-reagent complex was diluted with Opti-MEM and added to one well of cells in a 6-well plate prewashed with Opti-MEM. Cells were placed back on fresh full medium 4–6 h after transduction. One or 2 days before tau PFF transduction, inducible cells were placed on medium containing 1 μg/ml of Dox to ensure high expression of soluble tau by the time of transduction. For generating monoclonal cells with persistent tau aggregates, clone 4 cells with inducible expression of T40/P301L-GFP were plated 1 day before tau PFF transduction with 100 ng/ml of Dox. Following tau PFF transduction, clone 4 cells were maintained on 100 ng/ml of Dox and cultured for 3 weeks with regular passaging. Monoclonal cell lines with close to 100% aggregation rate, including clone 4.1 cells, were generated by limited dilution.

Sorting of Clone 4.1 Cells—To enrich for cells carrying large compact tau aggregates, the T40/P301L-GFP aggregate-bearing monoclonal line 4.1 was sorted using a FACS Aria flow cytometer (BD Biosciences) and FACS Diva 6.0 software. Cell sorting was based on the morphology of GFP-positive tau inclusions, which were differentiated based on the height and width of the GFP signals (FITC-H and FITC-W, respectively, as shown in Fig. 1*D*). The width of the signals (in arbitrary units) indicates the "duration" of the fluorescent signal while a cell passes through the laser, and the height of the signals (in arbitrary units) indicates signal intensity. In cells without tau aggregates or with only small tau aggregates, GFP signals are evenly distributed over the entire cells and are therefore characterized by a larger signal width as compared with cells with large and more consolidated aggregates. Gates for sorting aggregate-carrying cells were set at the extreme values of the FITC-W spectrum to enrich for cells with the sharpest width and hence the largest aggregates (see Fig. 1*D*). To confirm the accuracy of sorting, sorted clone 4.1 cells were fixed and stained with APC-conjugated AT8 antibody, which specifically recognizes phosphorylated tau aggregates. Sorted clone 4.1 cells were used in this study and were referred to as clone 4.1 for simplicity.

Reinstatement of Tau Aggregates in Clone 4.1 Cells—Clone 4.1 cells were grown in the absence of Dox for various intervals (0, 4, 7, 14, and 21 days) to allow for clearance of both soluble and insoluble tau. Cells were then split onto clear bottom 384-well plates and re-exposed to Dox for different intervals (0, 2, 4,

TABLE 1
Antibodies used in the study

Antibody	Specificity	Host species	Dilution	Source or Ref.
17025	Raised against human recombinant tau	Rabbit	1:1000 (WB)[a]	52
PHF-1	*p*-Tau (phosphorylated at Ser-396 and Ser-404)	Mouse	1:1000 (WB), 1:2000 (ICC)	Gift from Dr. Peter Davies
AT8	*p*-Tau (phosphorylated at Ser-202 and Thr-205)	Mouse	1:500 (ICC)	Innogenetics
GAPDH (6C5)	Glyceraldehyde-3-phosphate dehydrogenase	Mouse	1:3000 (WB)	Advanced Immunochemical
PM036	LC3	Rabbit	1:500 (WB) 1:2000 (ICC)	MBL
2C11	p62	Mouse	1:1000 (ICC)	Abnova
610832	P62	Mouse	1:1000 (WB)	BD Transduction
H4A3	LAMP1	Mouse	1:1000 (ICC)	BD Biosciences
Ub1b4	Ubiquitin	Mouse	1:1000 (WB), 1:1000 (ICC)	53
PW8155	20S proteasome	Rabbit	1:2000 (ICC)	Biomol
81A	*p*-α-Syn (phosphorylated at Ser-129)	Mouse	1:5000 (ICC)	54
MJF-R13	*p*-α-Syn (phosphorylated at Ser-129)	Rabbit	1:2000 (ICC)	Michael J. Fox Foundation

[a] WB, Western blotting; ICC, immunocytochemistry.

and 7 days) to reinitiate aggregate formation, with 16 wells per condition. To assess the amount of insoluble tau harbored by cells at the end of the experiment, cells were extracted with 1% hexadecyltrimethylammonium bromide (Sigma) and then fixed with 4% paraformaldehyde (PFA). The plate was imaged using InCell 1000 (GE Healthcare) with 4 images taken per well, and GFP signals were quantified using Developer 1.9 software (GE Healthcare) and expressed as average area/nucleus.

Induction of α-Synuclein (α-Syn) Aggregates in Clone 4.1 Cells—Clone 4.1 cells grown in Dox-containing medium were plated 1 day before transient transfection with A53T mutant α-Syn in pcDNA5/TO using FuGENE® 6 according to the manufacturer's instructions at 2 μg of DNA per well for cells on a 6-well plate. C-terminal truncated α-Syn (1–120) with a myc-tag was purified, assembled into fibrils, and transduced as previously described, whereby 0.8 μg of Myc-syn1–120 PFFs were transduced per well with Bio-PORTER reagent (24). At ~6 h after transduction, cells were placed back on complete medium containing 1 μg/ml of Dox. Robust induction of Lewy body-like α-Syn aggregates was observed 1–2 days after PFF transduction.

Preparation of Lysosomal and Proteasomal Inhibitors—Stock solutions of bafilomycin A1 (BafA1) (Sigma), clasto-lactacystin β-lactone (c-lac) (Calbiochem), and epoxomicin (epox) (Sigma) were prepared at 0.1, 3, and 2.5 mg/ml, respectively, in DMSO, aliquoted and kept frozen at −20 °C until use. Stock solution of chloroquine diphosphate (CQ) (Sigma) was freshly prepared at 30 mM in distilled H_2O right before each experiment. Further dilutions of these drugs were directly made in cell medium to reach working concentrations as indicated in the figure legends.

Immunocytochemistry and Imaging—For regular fixing (as shown in Fig. 1*B, left panel*), cells were incubated with ice-cold 4% PFA for 15 min at room temperature. To remove soluble proteins (as shown in Fig. 1*B, right panel*), 1% Triton X-100 was added to 4% PFA during fixing. After blocking with 3% bovine serum albumin and 3% FBS in phosphate-buffered saline (PBS) for 1 h at room temperature, cells were incubated with specific primary antibodies (see Table 1) diluted in the blocking buffer for 2 h at room temperature or overnight at 4 °C, followed by incubation with Alexa Fluor 594- or 647-conjugated secondary antibodies (Invitrogen) diluted in the blocking buffer for 2 h at room temperature. For immunostaining of LC3 and LAMP1, cells were fixed with 4% PFA without Triton X-100, but 0.05% saponin was added to the blocking buffer for all the subsequent blocking and antibody incubation steps. Stained coverslips were mounted onto glass slides using DAPI-containing Fluoromount-G (Southern Biotech). DAPI-free Fluoromount-G was used for coverslips stained with Alexa Fluor 647-conjugated secondary antibody. Immunofluorescence images were acquired using an Olympus BX 51 microscope equipped with a digital camera DP71 and DP manager (Olympus), or Leica DMI6000 microscope equipped with a DFC365 FX monochrome camera and Leica Application Suite (Leica), or Axiovert 135 microscope with a AxioCam MRm camera. All live imaging was performed using a Leica DMI6000 microscope, with cells grown in the regular medium and the culture dish secured inside a moist chamber maintained at 37 °C.

Whole Coverslip Quantifications of Triton-insoluble Tau Aggregates during Dox Withdrawal—To test whether soluble tau removal indeed led to progressive reduction in the total aggregate burden independent of mitosis-mediated aggregate dilution, clone 4.1 cells that had been off Dox for 5 days were plated at 4×10^4 per coverslip on a 24-well plate for quantifying the amounts of Triton-insoluble tau aggregates over time. Two coverslips were fixed at ~5 h after plating for the 5-day off Dox time point. Two more sets of duplicate coverslips were fixed at 7 and 10 days off Dox with no further passaging of the cells during the 5-day period. Fixing was done with 4% PFA containing 1% Triton X-100 to remove soluble tau. Automated scanning of whole coverslips were then performed using a Lamina™ Multilabel Slide Scanner (PerkinElmer Life Sciences) to capture Triton-resistant GFP signals, which mark insoluble tau aggregates. The total intensity of GFP signals (total area occupied × average intensity) were quantified using the image analysis platform HALO™ (Indica labs).

Sequential Extraction and Western Blotting—Cells were first scraped into Triton lysis buffer (1% Triton X-100 in 50 mM Tris, 150 mM NaCl, pH 7.6) containing protease and phosphatase inhibitors and incubated on ice for 15 min. Following sonication, lysates were centrifuged at 100,000 × *g* for 30 min at 4 °C. Supernatants were kept as "Triton fraction," whereas pellets were washed once in Triton lysis buffer (again with sonication and centrifugation), resuspended, and sonicated in SDS lysis buffer (1% SDS in 50 mM Tris, 150 mM NaCl, pH 7.6) containing protease and phosphatase inhibitors at a volume that is ⅓ or ¼ of the Triton lysis buffer. After centrifugation at 100,000 × *g* for

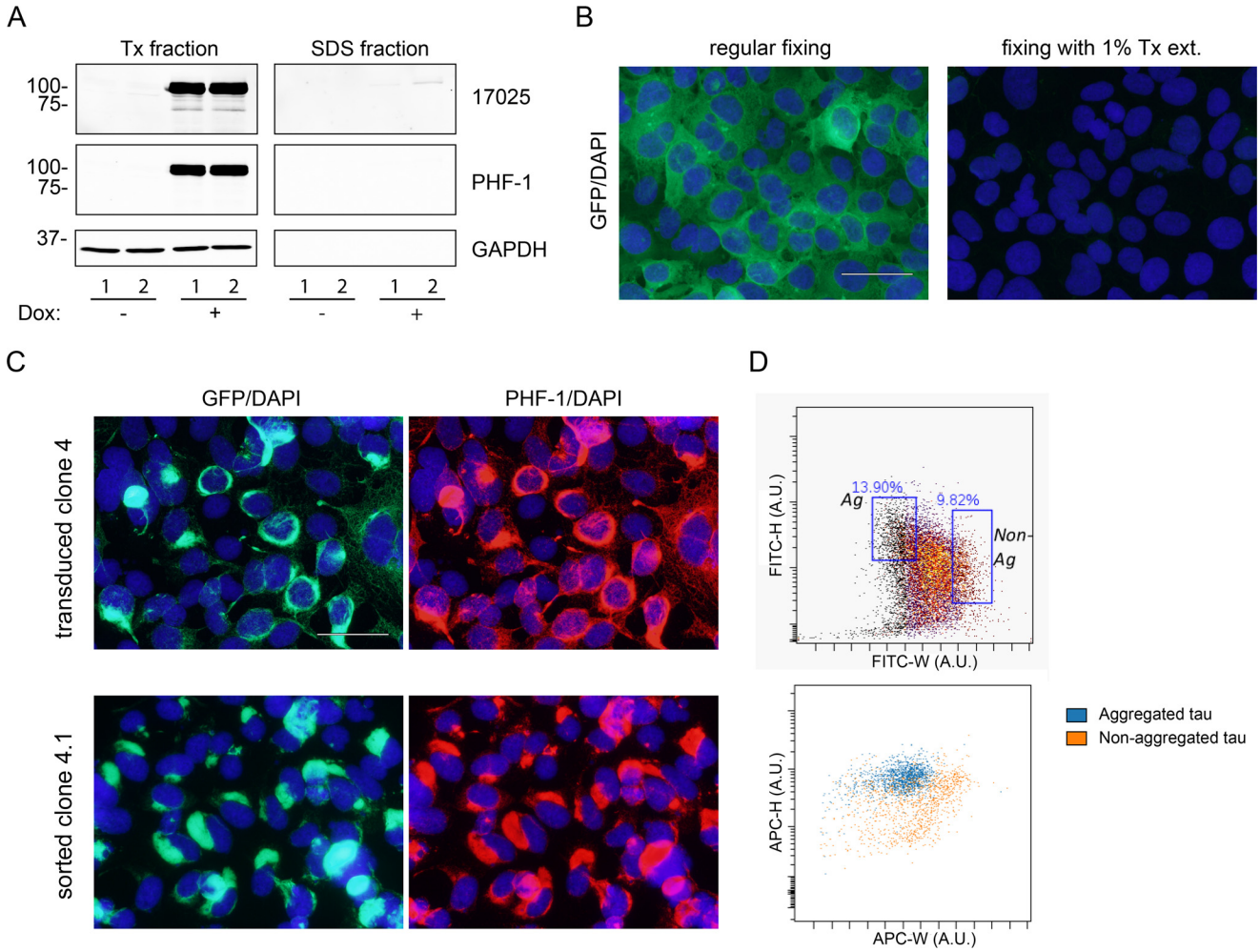

FIGURE 1. **Generation of a stable clone persistently carrying tau aggregates.** A, a monoclonal cell line with Dox-regulated expression of T40/P301L-GFP (clone 4) was sequentially extracted by 1% Triton X-100 lysis buffer (*Tx*) followed by 2% SDS lysis buffer and immunoblotted with a polyclonal pan-tau antibody 17025 and phospho-tau antibody PHF-1 (pS396/S404). GAPDH was used as the loading control. Little tau expression was observed in cells grown in Dox-free medium (−). Although abundant tau expression was detected after 2 days induction with 1 μg/ml of Dox (+), no appreciable Triton-insoluble tau was recovered in the SDS fraction. *B*, in clone 4 cells that are induced with Dox, GFP-tagged tau remained largely soluble and can be completely removed by 1% Triton X-100 extraction during fixing (*1% Tx ext.*). Cells were counterstained with DAPI to visualize cell nuclei. *C*, *top panels*: Triton-insoluble tau accumulated in Dox-induced clone 4 cells after transduction of Myc-K18/P301L PFFs mediated by BioPORTER reagent; *bottom panels*, a monoclonal cell line stably carrying tau aggregates (*clone 4.1*) was generated after 3-week passaging and subcloning of Myc-K18/P301L PFF-transduced clone 4 cells followed by fluorescence-activated cell sorting. As in *B*, soluble proteins were extracted by 1% Triton X-100 during fixing. GFP-tagged tau aggregates (*left column*) also showed immunoreactivity for PHF-1 (*right column*). *D*, *top panel*, clone 4.1 cells were sorted based on GFP signals as described under "Experimental Procedures." About 13.9% of cells were selected as positive for aggregates (*Ag*), and about 9.82% as negative for aggregates (*Non-Ag*). The two categories of cells were separately cultured after sorting. *Bottom panel*: immunostaining with APC-conjugated AT8 antibody (specific for tau phosphorylated at Ser-202/Thr-205) showed that cells located within the Ag gate based on the GFP signals (*blue dots*) are characterized by lower APC-W signals (in *A.U.*, arbitrary units), corresponding to more condensed punctuate aggregates, as compared with the more diffuse distribution with higher APC-W signals for cells in the Non-Ag gate (*orange dots*). *Scale bars*: 50 μm for *B* and *C*.

30 min at 22 °C, supernatants were saved as "SDS fraction." Protein concentrations in the Triton fraction were determined using the bicinchoninic acid assay (Fisher). Five to 15 μg of proteins from the Triton fraction and an equal volume of corresponding SDS fraction were resolved on 5–20% SDS-polyacrylamide gels, transferred to nitrocellulose membranes, and blocked in 5% fat-free milk in Tris-buffered saline before probing with specific primary antibodies (see Table 1). Odyssey blocking buffer (Li-Cor Biosciences) was used for LC3 blots. The blots were further incubated with IRDye-labeled secondary antibodies and scanned using ODY-2816 Imager (Li-Cor Biosciences).

Quantifications and Statistical Analysis—Densitometry quantification for Western blotting was performed using Odyssey software (Li-Cor Biosciences). For quantifying the percentage of tau aggregate-bearing cells, 10 random field images were taken at ×40 magnification per time point for each independent set of experiment, and the counting was done manually using the "Cell Counter" plug-in in ImageJ (NIH). Colocalization between tau or α-Syn aggregates and ALP or UPS markers was quantified by Manders coefficients using the "JACoP" plug-in in ImageJ with the threshold for each channel manually adjusted to remove background signals. Ten ×40 random-field images from each independent set of experiments were included for the colocalization analysis. For all of the above, the numbers of independent experiments conducted were indicated in the figure legends. Statistical analyses were performed as described in the figure legends. For comparing tau levels

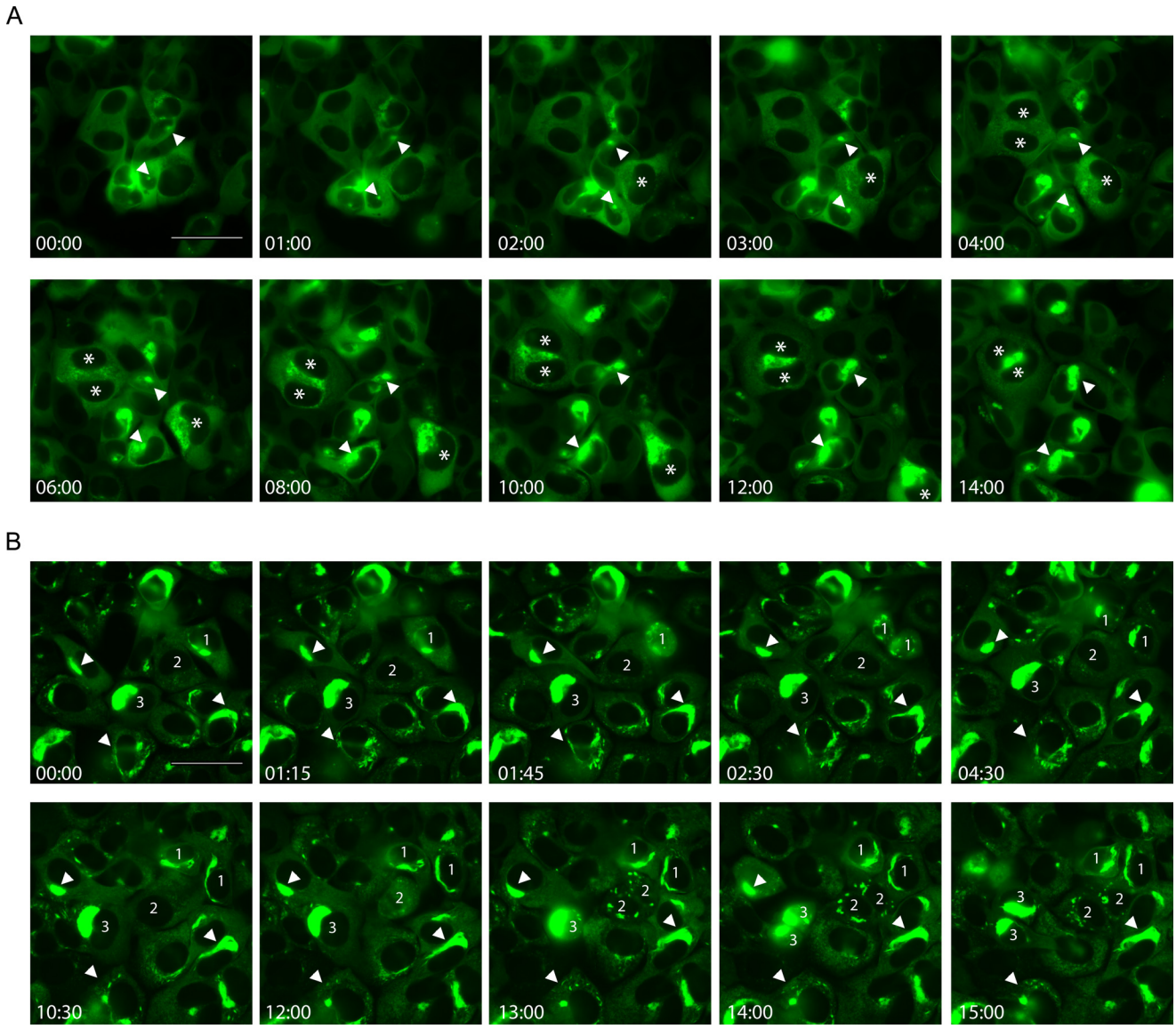

FIGURE 2. **The dynamics of tau aggregates.** *A*, selected snapshots from live imaging of clone 4 cells starting at 6–7 h after transduction of tau PFFs. *Arrowheads* point to examples of small focal inclusions developing into large aggregates, whereas *stars* mark examples of cells initially harboring diffuse aggregates. See supplemental Movie S1 for the complete time-lapse video. *B*, selected snapshots from live imaging of clone 4.1 cells with persistent tau aggregates. Numbers *1–3* mark examples of dividing cells. *Arrowheads* point to examples of aggregates showing morphological reorganization. See supplemental Movie S2 for the complete time-lapse video. Relative timing of the snapshots was presented as hh:mm. *Scale bars*: 50 μm.

during Dox removal (Fig. 3, *C* and *D*), two-way ANOVA was performed followed by Dunnett's post hoc test comparing each off Dox time point with $t = 0$. For analyzing total intensity of tau aggregate during Dox removal (Fig. 4*B*), one-way ANOVA was performed followed by Tukey's post hoc test for all pairwise comparisons. For analyzing the effects of lysosomal and proteasomal inhibitors on tau clearance in clone 4.1 cells (Fig. 6), one-way ANOVA was performed followed by Dunnett's post hoc test comparing each drug treatment condition with the untreated control. For the other experiments, *a priori* pairwise comparisons were conducted using two-tailed unpaired Student's *t* test, with the selected comparisons for each experiment described in the figure legends. For all statistical analysis, differences with *p* values less than 0.05 are considered significant and marked with "*" in the graphs.

Results

Generation of Tau Aggregate-bearing Cells Using an Inducible Cell Line—To investigate the turnover of tau aggregates in cells, we generated a monoclonal line of QBI-293 cells (clone 4 cells) with Dox-regulated inducible expression of human tau of the longest isoform carrying the P301L mutation (T40/P301L) (Fig. 1*A*), with a GFP tag attached to facilitate direct visualization of tau inclusions (Fig. 1*B*). The overexpressed mutant tau in clone 4 cells remains soluble and fully extractable by 1% Triton X-100 (Fig. 1, *A* and *B*). To induce tau aggregation, clone 4 cells were transduced with tau PFFs assembled from recombinant Myc-K18/P301L using BioPORTER reagent, as previously described (18). Triton-insoluble tau aggregates were robustly induced after tau PFF transduction when tau expression was turned on (Fig. 1*C, top panels*), suggesting seeded fibrillization

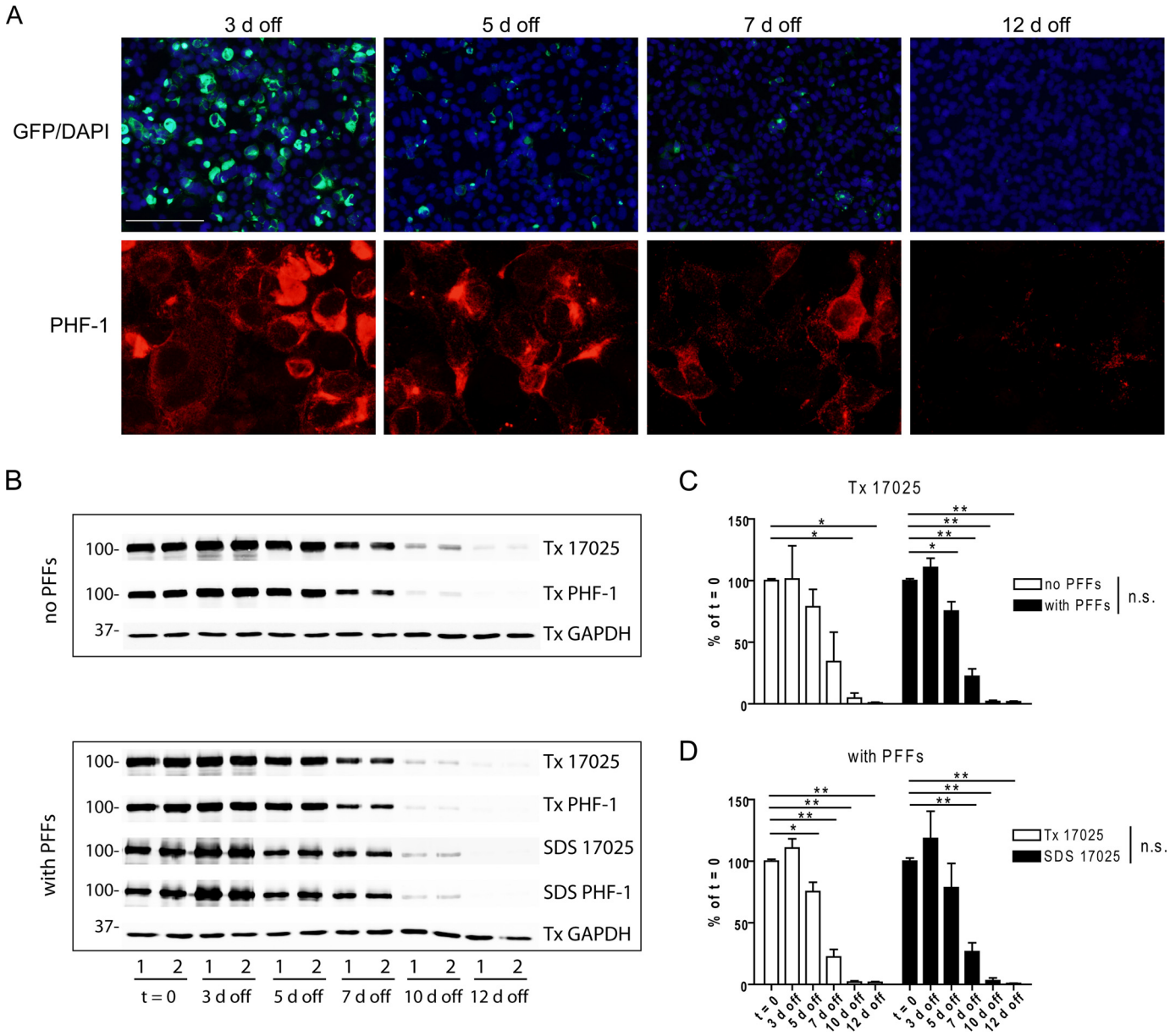

FIGURE 3. **Clearance of tau aggregates in tau PFF-transduced clone 4 cells following suppression of soluble tau expression.** *A*, Triton-insoluble tau aggregates were shown at different time points after tau PFF-transduced clone 4 cells were cultured on Dox-free medium (3 to 12 days off Dox). Soluble proteins were removed by 1% Triton X-100 extraction during fixing. *Scale bar*: 200 μm for GFP; 50 μm for PHF-1. *B*, clone 4 cells with or without tau PFF transduction were sequentially extracted by 1% Triton X-100 lysis buffer (*Tx*) followed by 2% SDS lysis buffer (*SDS*) after different off Dox durations and immunoblotted with 17025 and PHF-1. Only the Triton X-100 fraction was shown for cells without tau PFF transduction as these cells do not contain Triton X-100-insoluble tau (see Fig. 1*A*). GAPDH served as a loading control; "$t = 0$" refers to the time point right before Dox removal. Samples from duplicate wells of a representative set of experiments were shown as *1* and *2*. *C* and *D*, densitometry quantifications of 17025 immunoblots for experiments shown in *B*. Independent sets of experiments used for quantification: $n = 2$ for "no PFFs" cells; $n = 4$ for "with PFFs" cells, but only 2 sets of experiments had 10-day off time points, and 3 sets had 12-day off time points. Measurements were normalized to $t = 0$ samples in each set and shown as mean ± S.E. *C* compares clearance of Triton X-100-soluble tau in cells with and without tau PFF transduction, whereas *D* compares clearance of Triton X-100-soluble and -insoluble (*i.e.* SDS-soluble) tau in cells with PFF transduction. For both *C* and *D*, two-way ANOVA showed a significant effect of time on tau levels ($p < 0.0001$) but a non-significant difference between no PFFs and with PFFs cells or between Triton X-100-soluble and -insoluble tau in PFF-transduced cells. Dunnett's post hoc test was performed for pairwise comparisons between $t = 0$ and each of the other time points, with significant differences marked in the graphs. *, $p < 0.05$. **, $p < 0.01$. Quantification of PHF-1 blots revealed similar trends (data not shown). *n.s.*, non-significant.

of P301L mutant tau is minimally affected by the presence of a GFP tag. Live imaging was performed on newly transduced clone 4 cells to delineate the early phase of tau PFF-seeded aggregation in real time (supplemental Movie S1; Fig. 2*A*). At about 6–7 h after the addition of tau PFFs, a subset of cells displayed small focal tau inclusions that gradually increased in size over time, presumably reflecting recruitment of soluble tau into growing aggregates. Other cells started with less discrete and more diffusely distributed puncta, which progressively became more prominent and eventually coalesced into one or two large aggregates per cell.

To create a homogeneous clonal population of tau aggregate-bearing cells, we passaged clone 4 cells, in which aggregates had formed after tau PFF transduction, for 3 weeks,

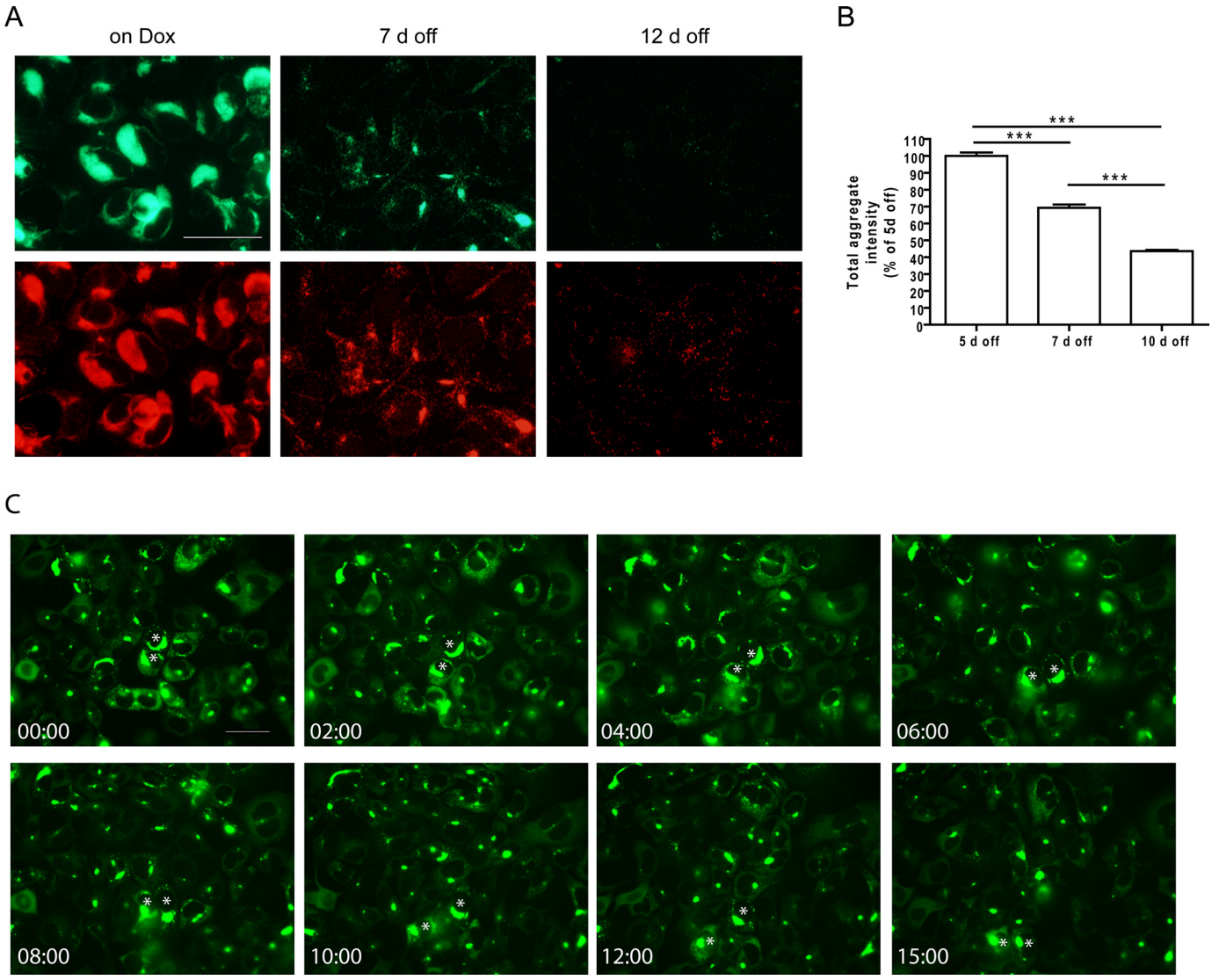

FIGURE 4. **Clearance of tau aggregates in clone 4.1 cells following suppression of soluble tau expression.** A, Triton-insoluble tau aggregates labeled by GFP signals (*top panels*) and PHF-1 immunostaining (*bottom panels*) in clone 4.1 cells maintained on Dox or at 7 or 12 days off Dox. *Scale bar*, 50 μm. *B*, whole coverslip quantifications for the total intensity of Triton-insoluble GFP-positive tau aggregates in clone 4.1 cells at 5, 7, and 10 days off Dox. Cells were plated onto the coverslips at 5 days off Dox and no further passaging was performed thereafter. Three independent sets of experiments were performed, with the total aggregate intensity measurements normalized to that of 5 days off Dox within each set of experiment. Data are shown as mean ± S.E. One-way ANOVA was performed followed by Tukey's post hoc test for all pairwise comparisons. ***, $p < 0.001$. *C*, selected snapshots from live imaging of clone 4.1 cells from 4 days off Dox to 5 days off Dox. *Stars* mark examples of large and elongated aggregates getting consolidated into smaller round inclusions. See supplemental Movie S3 for the complete time-lapse video. Relative timing of the snapshots was presented as hh:mm. *Scale bar*, 50 μm.

followed by single cell cloning to generate monoclonal cell lines. Notably, we obtained clones with persistent tau inclusions. One of these clones, clone 4.1, was further sorted to enrich for cells with relatively large aggregates (Fig. 1, *D* and *C*, *bottom panels*). About 95% of sorted clone 4.1 cells (hereafter referred to as clone 4.1 for simplicity) maintained tau aggregates even after more than 100 days of passaging in culture, implying that tau inclusions can be faithfully propagated during mitosis and cells carrying aggregates must be dividing at a similar rate as aggregate-free cells in our system. Live imaging of clone 4.1 cells (supplemental Movie S2; Fig. 2*B*) indeed demonstrated that aggregated tau was readily and reliably segregated into daughter cells during mitosis, which sometimes required remodeling of chunky aggregates into finer pieces to be inherited by daughter cells, wherein further recruitment and coalescence occurred. In cells not actively dividing, tau aggregates are also dynamic structures that are free to undergo morphological changes, and highly mobile small aggregates frequently appear to be dissociating from larger aggregates (supplemental Movie S2).

Clearance and Re-emergence of Tau Aggregates Upon Modulation of Soluble Tau Expression—Two days after tau PFF transduction, clone 4 cells were placed on Dox-free medium to turn off soluble tau expression. Although abundant Triton-insoluble tau aggregates remained after 3 days off Dox (Fig. 3*A*), probably because of delayed reduction in soluble tau (Fig. 3, *B* and *C*), a prominent decrease in Triton-insoluble tau started at 5 days off Dox until only minute quantities of small aggregates could be detected at 12 days off Dox (Fig. 3*A*). Immunoblotting of sequentially extracted cell lysates with antibodies against total

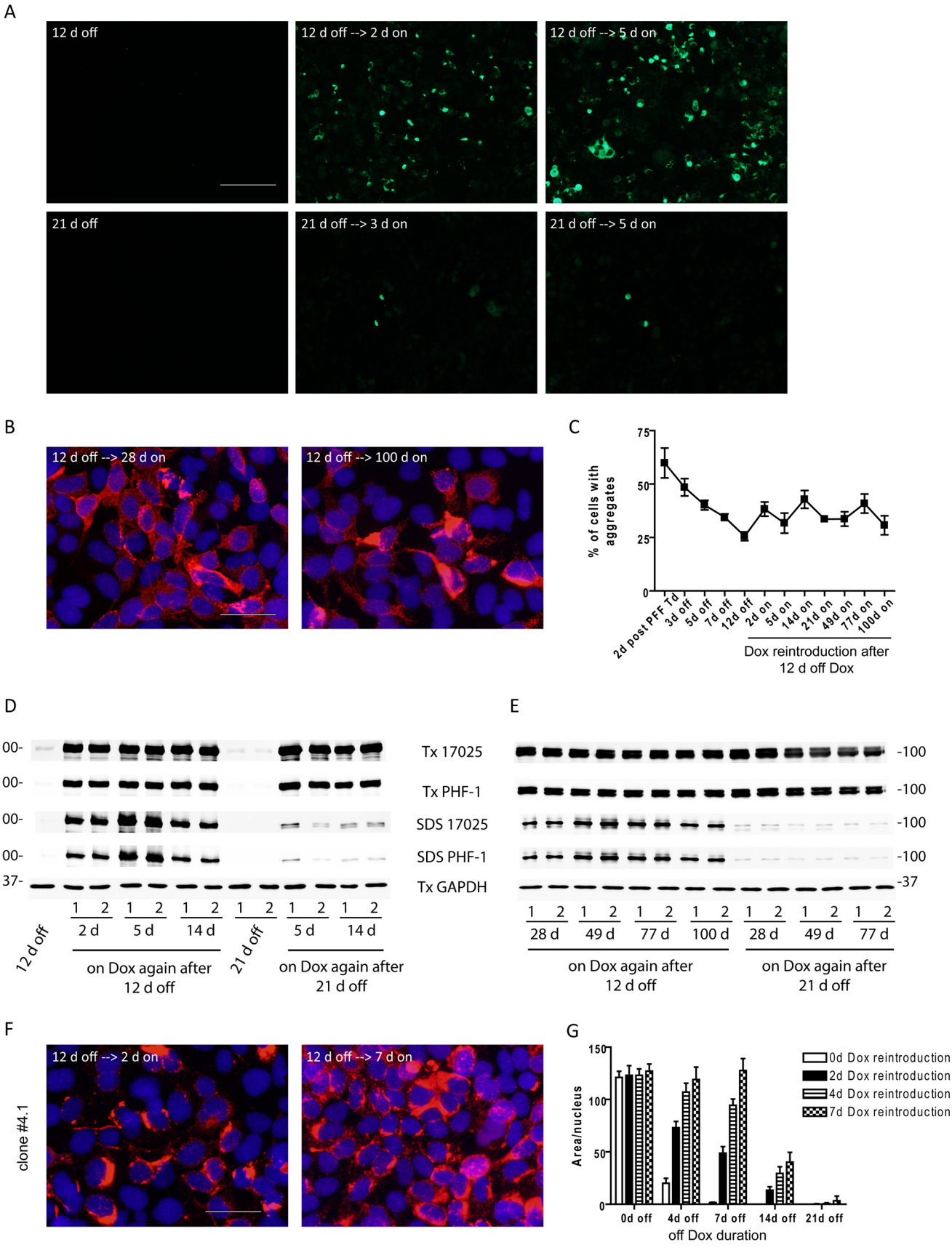
A
12 d off
12 d off --> 2 d on
12 d off --> 5 d on
21 d off
21 d off --> 3 d on
21 d off --> 5 d on
B
12 d off --> 28 d on
12 d off --> 100 d on
C
% of cells with aggregates
75
50
25
0
2d post PFF
1d
3d off
5d off
7d off
12d off
2d on
5d on
14d on
21d on
49d on
77d on
100d on
Dox reintroduction after 12 d off Dox
D
100-
100-
100-
100-
37-
Tx 17025
Tx PHF-1
SDS 17025
SDS PHF-1
Tx GAPDH
1 2 1 2 1 2 1 2 1 2 1 2
2 d
5 d
14 d
5 d
14 d
12 d off
21 d off
on Dox again after 12 d off
on Dox again after 21 d off
E
-100
-100
-100
-100
-37
1 2 1 2 1 2 1 2 1 2 1 2 1 2
28 d
49 d
77 d
100 d
28 d
49 d
77 d
on Dox again after 12 d off
on Dox again after 21 d off
F
clone #4.1
12 d off --> 2 d on
12 d off --> 7 d on
G
Area/nucleus
150
100
50
0
0d Dox reintroduction
2d Dox reintroduction
4d Dox reintroduction
7d Dox reintroduction
0d off
4d off
7d off
14d off
21d off
off Dox duration

tau (17025) and phosphorylated tau (PHF-1) showed that reduction in Triton-insoluble tau mirrors reduction in Triton-soluble tau (Fig. 3, *B* and *D*), suggesting that cells are capable of clearing aggregated tau when depleted of the substrate (*i.e.* soluble tau) for templated recruitment. Moreover, the presence of tau aggregates did not significantly influence the clearance of soluble tau (Fig. 3, *B* and *C*).

A similar trend of aggregate reduction was observed in clone 4.1 cells upon withdrawal of Dox (Fig. 4*A*). To confirm that the apparent clearance of tau pathology cannot be solely attributed to continual dilution of aggregates by cell division, whole coverslip quantifications of Triton-insoluble GFP signals were performed on clone 4.1 cells, which revealed a steady reduction in the total burden of tau aggregates at the population level from 5 to 10 days off Dox (Fig. 4*B*). Live imaging of clone 4.1 cells off Dox further showed that large and sometimes elongated tau aggregates gradually turned into smaller round inclusions over time, with fine pieces of aggregates appearing to be dissociating from the former (supplemental Movie S3; Fig. 4*C*). Interestingly, the tiny thread-like aggregates seem to be extremely mobile entities exhibiting visible displacement within a fraction of a second (supplemental Movie S4).

To test whether cells grown in Dox-free medium for a prolonged period of time will be repopulated with tau aggregates when tau expression is turned on again, we returned transduced clone 4 cells to Dox-containing medium after either 12 or 21 days off Dox. Following 12 days of suppressed tau expression, reintroduction of soluble tau resulted in rapid reinstatement of robust tau aggregation within 2 days (Fig. 5, *A, top panels*, and *D*). Moreover, these re-emerged aggregates were stably propagated for up to 100 days as long as soluble tau was being expressed (Fig. 5, *B* and *E*). Quantification of the percentage of aggregate-bearing cells (Fig. 5*C*) revealed a steady decline in the prevalence of aggregates as tau expression was turned off, but about 25% of cells still retained small amounts of aggregates at 12 days off Dox, which are only visible under high magnification (Fig. 3*A*), and abundant tau aggregates re-appeared and were sustained in a similar percentage of cells after tau expression was turned on again. The re-emergence of tau inclusions following 12 days Dox withdrawal and reintroduction similarly occurred in clone 4.1 cells (Fig. 5*F*), in which BioPORTER reagent and cell membrane-associated tau PFFs must have been long cleared after weeks of passaging in culture.

However, when the Dox withdrawal period was increased to 21 days for PFF-transduced clone 4 cells, very few cells re-developed conspicuous aggregates following the reintroduction of Dox (Fig. 5, *A, bottom panels*, and *D* and *E*). Such "off time"-dependent reinstatement of tau aggregates was also observed in clone 4.1 cells, whereby full recovery of extensive tau aggregation occurred when the off Dox period was limited to 7 days, whereas longer suppression of tau expression led to either partial or no recovery (Fig. 5*G*). These results suggest cells that retain aggregated tau after varying clearance durations are the ones that eventually regain full pathology once soluble tau is available again to be recruited by the remnant seeds. The longer the suppression of soluble tau expression, the lower the percentage of cells maintaining seeds.

Conditional Degradation of Tau Aggregates by Autophagy—To examine whether cellular protein degradation systems are playing any role in the clearance of tau aggregates when soluble tau expression is turned off, clone 4.1 cells were treated with pharmacological inhibitors of lysosome function (chloroquine diphosphate or CQ; bafilomycin A1 or BafA1) or proteasome function (clasto-lactacystin β-lactone or c-lac; epoxomicin or epox) from 3 days off Dox to 5 days off Dox, during which Triton-soluble and -insoluble tau decreased by about 67 and 50%, respectively (Fig. 6, *A*–*C*). Both CQ and BafA1, which prevent acidification of lysosomes, resulted in dramatic accumulations of LC3-II (lipidated form of LC3 specifically localized in the autophagosomal membranes), indicating successful blockade of lysosomal degradation (25) (Fig. 6*D*). Both c-lac and epox led to increased accumulations of high molecular weight ubiquitinated proteins in the Triton-soluble fraction, supporting inhibition of the UPS. Proteasomal inhibition by c-lac or epox was also associated with increased LC3-II levels, which could be due to a compensatory activation of autophagy, as shown before (15).

Immunoblotting of sequentially extracted cell lysates at 5 days off Dox showed significantly higher levels of Triton-insoluble tau resulted from treatment of lysosomal inhibitors, but no significant difference was found with proteasomal inhibition as compared with untreated cells (Fig. 6, *D*, *F,* and *G*). This suggests lysosomes, but not proteasomes, play a role in the clearance of aggregated tau, although inhibition of lysosomes did not completely restore insoluble tau to the pre-treatment levels (compare Fig. 6, *C* and *F*), arguing other mechanisms may be at play (see "Discussion"). Parallel experiments were performed on clone 4.1 cells maintained on Dox, but inhibition of neither lysosomes nor proteasomes led to significant elevation of Triton-insoluble tau, indicating less efficient degradation of tau aggregates when soluble tau is abundant (Fig. 6, *H*, *J,* and *K*). On the other hand, we noted that proteasomal inhibitors only resulted in significantly higher levels of soluble tau in cells maintained on Dox (Fig. 6, *E* and *I*). Their lack of effect in cells off Dox could be explained by a compensatory takeover of the

FIGURE 5. **Re-emergence and long-term propagation of tau aggregates after restoration of soluble tau expression.** *A*, Triton-insoluble tau aggregates visualized by GFP signals were shown for 2 paradigms of Dox removal (12 or 21 days off Dox) followed by different incubation times after the reintroduction of Dox to the cell medium. *Scale bar*, 200 μm. *B*, Triton-insoluble tau aggregates recognized by PHF-1 (*red*) continued to accumulate in a subset of cells up to 100 days after soluble tau expression was restored following 12 days off Dox. *Scale bar*, 50 μm. *C*, quantification of the percentage of tau aggregate-bearing cells upon modulation of soluble tau expression in tau PFF-transduced clone 4 cells. "*2 d post-PFF Td*" refers to 2 days after the transduction of tau PFFs right before cells were withdrawn from Dox. Data are shown as mean ± S.E. based on 3 independent sets of experiments. *D* and *E*, immunoblotting of sequentially extracted cell lysates (*Tx*: 1% Triton X-100 lysis buffer; *SDS*, 2% SDS lysis buffer) from tau PFF-transduced clone 4 cells at different time points after cells were placed back on Dox-containing medium following either 12 or 21 days off Dox. Samples from duplicate wells of a representative set of experiment were shown as *1* and *2*. *F*, Triton-insoluble tau aggregates (PHF-1 in *red*) similarly re-emerged in clone 4.1 cells after Dox reintroduction. *Scale bar*, 50 μm. *G*, differential re-emergence of tau pathology in clone 4.1 cells with different off Dox durations followed by different durations of Dox reintroduction. The extent of tau pathology was scored as the area occupied by GFP signals normalized to nuclear count with soluble protein extracted during fixing. Results from one set of experiments are shown here as mean ± S.D., whereby each *bar* represents readings from 16 replicate wells.

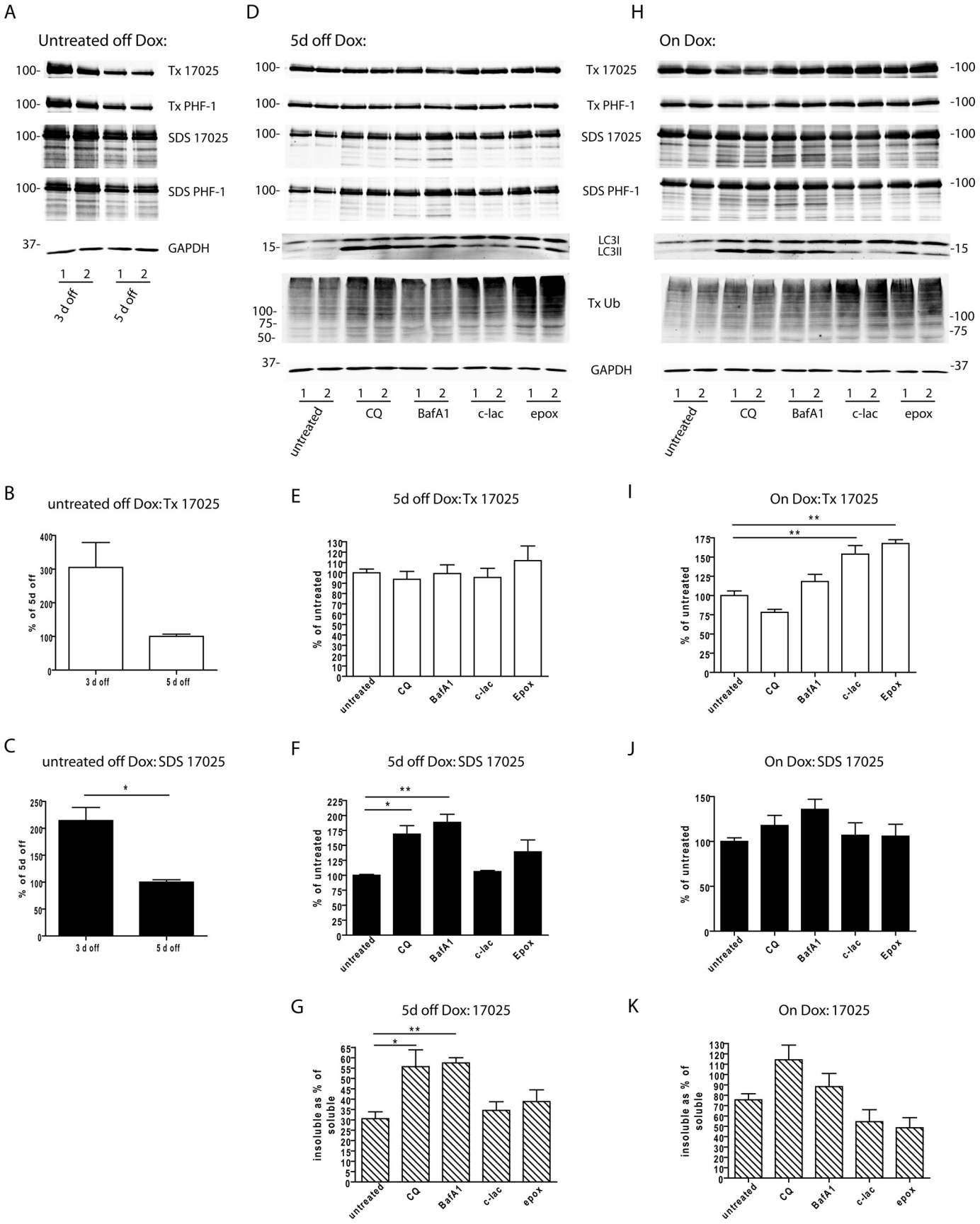
A
Untreated off Dox:
100-
Tx 17025
Tx PHF-1
SDS 17025
SDS PHF-1
37-
GAPDH
1 2 1 2
3 d off
5 d off
D
5d off Dox:
15-
LC3I
LC3II
Tx Ub
75-
50-
untreated
CQ
BafA1
c-lac
epox
H
On Dox:
-100
-15
-75
-37
B
untreated off Dox: Tx 17025
% of 5d off
3 d off
5 d off
E
5d off Dox: Tx 17025
% of untreated
untreated
CQ
BafA1
c-lac
Epox
I
On Dox: Tx 17025
C
untreated off Dox: SDS 17025
F
5d off Dox: SDS 17025
J
On Dox: SDS 17025
G
5d off Dox: 17025
insoluble as % of soluble
K
On Dox: 17025

autophagy, which has been shown to be capable of degrading soluble tau (14) but conceivably becomes overwhelmed when soluble tau level is too high.

Interactions between Tau Aggregates and Autophagy Markers—Lysosomes are the final degradation machinery of autophagy pathways, which include macroautophagy, microautophagy, and chaperon-mediated autophagy (reviewed by Ref. 26). Given the physical size of tau aggregates, macroautophagy (hereafter referred to as autophagy for simplicity) is the most likely mechanism mediating the degradation of tau aggregates during Dox removal. Indeed, immunostaining for markers of autophagy in clone 4.1 cells revealed clusters of LC3 and p62 (an adaptor protein on the autophagosomes) puncta frequently around tau inclusions, suggesting recruitment of autophagosomes by tau aggregates (Fig. 7, *A* and *B*). However, no obvious difference in the extent of colocalization between tau inclusions and autophagosomes was observed in clone 4.1 cells on or off Dox, which was further confirmed by Manders coefficient analysis on the percentage area of tau inclusions (based on focal accumulation of GFP signals) with overlapping LC3 or p62 immunoreactivities (LC3: 23.8 ± 0.9% for off Dox, 31.6 ± 3.5% for on Dox, $p = 0.098$; p62: 27.1 ± 3.5% for off Dox, 20.0 ± 4.2% for on Dox, $p = 0.26$). Therefore, the insubstantial degradation of Triton-insoluble tau when cells are on Dox is unlikely due to failed interactions with autophagosomes *per se*. A more plausible reason is that tau aggregates may be too large to be properly handled by the autophagy system when soluble tau is highly expressed, whereas suppression of soluble tau expression promotes the formation of smaller aggregates (supplemental Movie S3; Fig. 4*C*), possibly through spontaneous disassembly as a result of shift in the equilibrium (27).

Even during Dox withdrawal, the degradation of tau aggregates seems to be an inefficient process. After a 1-day treatment with CQ, the dramatically increased LC3 and p62 accumulations, which presumably represent autophagolysosomes that failed to be turned over during the treatment period because of increased lysosomal pH, mostly did not colocalize with tau aggregates (Fig. 8*A* and *B*). In fact, Manders coefficients for the percentage area of LC3 or p62 immunoreactivities with overlapping tau aggregates were markedly lower in CQ-treated cells than in untreated cells either on or off Dox (Fig. 8*D* and *E*). These results suggest other cellular substrates were disproportionately more readily shuttled into autophagolysosomes for degradation as compared with tau aggregates. Therefore, frequent focal accumulations of LC3 and p62 around tau aggregates may actually represent stalled maturation of autophagosomes into autophagolysosomes or even inefficient packaging of tau aggregates into autophagosomes. Consistent with this idea, lack of clear colocalization of tau aggregates with lysosomes (labeled by LAMP1) was noted without (Fig. 7*C*) and with (Fig. 8*C*) CQ treatment, suggesting tau aggregates do not constitute a major pool of lysosomal substrates even when they do get degraded during the off Dox period.

The Effect of Tau Aggregation on Autophagy Flux—To investigate whether tau aggregates, either acutely induced in newly transduced clone 4 cells or persistently propagated in clone 4.1 cells, impair autophagy flux, cellular levels of LC3-II, p62, and Triton-insoluble high molecular weight ubiquitinated proteins were compared using Western blotting of lysates from Dox-induced clone 4 cells with and without tau PFF transduction (BioPORTER reagent treatment without tau PFFs serving as a control), clone 4.1 cells maintained on Dox, and clone 4.1 cells removed from Dox, with all cells treated either in the absence or presence of CQ (Fig. 9). Besides being functional components of the autophagy machinery, LC3-II and p62 themselves are also substrates of the ALP because they get degraded in the lysosomes alongside insoluble ubiquitinated proteins that cannot be degraded by the proteasomes (28). For all experimental groups, 2 days of lysosomal inhibition by CQ treatment led to tremendous accumulations of all three substrates (Fig. 9*A*). An estimation of turnover rates for the three substrates (level with CQ treatment, level without CQ treatment) revealed no significant difference among the different groups (Fig. 9, *E*–*G*), suggesting both acute and chronic exposures to tau aggregates have minimal effect on the cellular autophagy flux. Therefore, whereas tau aggregates are inefficiently handled by autophagy, they do not compromise the normal functioning of this degradation pathway, which is also supported by dramatic accumulation of LC3 and p62 upon CQ treatment shown by immunostaining (Fig. 8, *A* and *B*). Although tau aggregate-bearing cells tended to show enhanced steady-state LC3-II levels as compared with clone 4 cells expressing soluble tau without aggregates, the differences only reached statistical significance for clone 4.1 cells off Dox (Fig. 9*B*) and may represent a slight increase in LC3-II synthesis because LC3-II degradation was not affected (Fig. 9*E*). On the other hand, clone 4 cells newly transduced with tau PFFs displayed significant elevation in steady-state levels of p62 and insoluble ubiquitinated proteins (Fig. 9, *C* and *D*). Considering the largely normal turnover of autophagic substrates, this result suggests increased buildup of intracellular misfolded proteins (not just tau) immediately following induction of tau aggregation. Such proteostatic stress no

FIGURE 6. **Degradation of tau aggregates by autophagy pathway.** *A*, clone 4.1 cells that were 3 or 5 days off Dox were sequentially extracted with 1% Triton X-100 lysis buffer (*Tx*) followed by 2% SDS lysis buffer (*SDS*) and immunoblotted with 17025 and PHF-1. *B* and *C*, densitometry quantification of 17025 immunoblots as shown in *A* based on 2 independent sets of experiments. Student's *t* test was performed. *, $p < 0.05$. *D*, clone 4.1 cells were treated with pharmacological inhibitors of lysosomes (*CQ*: 30 μM chloroquine diphosphate; *BafA1*, 200 nM bafilomycin A1) or proteasomes (*c-lac*, 10 μM clasto-lactacystin β-lactone; *epox*, 20 nM epoxomicin) from 3 to 5 days off Dox and sequentially extracted. Immunoblotting with different antibodies was shown for one representative set of experiments, where *1* and *2* indicate samples from duplicate wells. Antibody against ubiquitin (*Ub*) revealed high molecular weight-ubiquitinated proteins. LC3 and GAPDH immunoblotting was only performed on the Triton X-100 fraction because they are fully extractable by 1% Triton X-100 lysis buffer. The LC3 antibody recognizes both LC3I (~18 kDa) and LC3-II (~14 kDa). *E*–*G*, densitometry quantification of 17025 immunoblots for experiments shown in *D*. *H*, the same experiment as shown in *D* was performed on clone 4.1 cells maintained on Dox. *I*–*K*, densitometry quantification of 17025 immunoblots for experiments shown in *H*. Quantifications were shown for Triton X-100-soluble tau (*E* and *I*), SDS-soluble tau (*F* and *J*), and SDS-soluble tau expressed as % of Triton X-100-soluble tau (*G* and *K*). As the volume of the SDS fraction is one-third of the volume of the Triton X-100 fraction for each biological sample, the amounts of tau in the SDS fraction measured from the immunoblots were divided by 3 for the calculation. For off Dox experiments: $n = 4$ independent experiments except for $n = 3$ for epox treatment group. For on Dox experiments: $n = 3$ independent experiments. Data are shown as mean ± S.E. One-way ANOVA was performed followed by Dunnett's post hoc test for pairwise comparisons between each drug treatment condition and the untreated control. *, $p < 0.05$. **, $p < 0.01$.

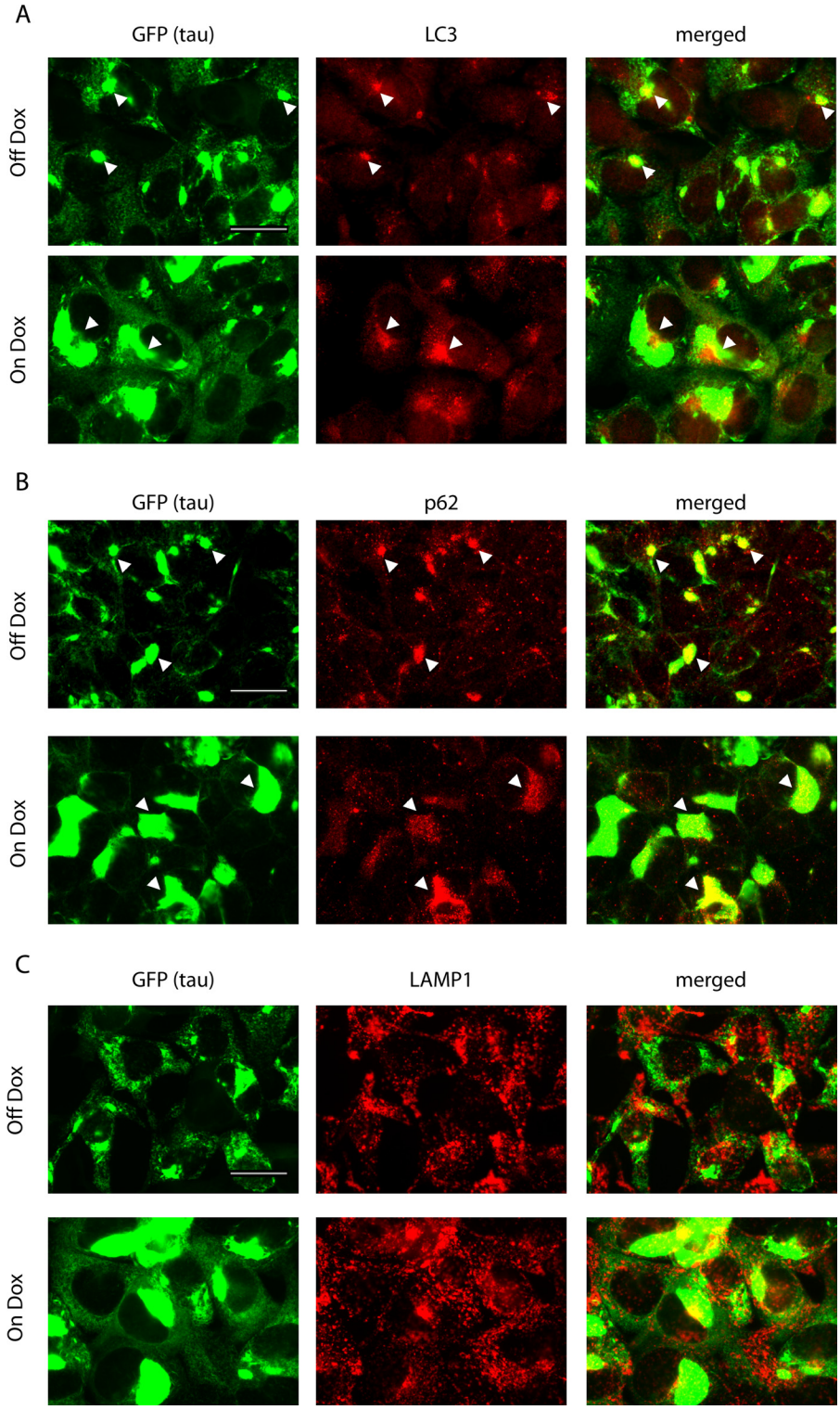

FIGURE 7. **Recruitment of autophagosomes by tau aggregates.** *A–C*, immunostaining of LC3, p62, and LAMP1 for clone 4.1 cells that were either removed from Dox for 4–5 days (*Off Dox*) or maintained on Dox (*On Dox*). Tau aggregates were visualized by GFP signals. *Arrowheads* point to examples of apparent colocalization or close physical association between tau aggregates and autophagosome markers. *Scale bars*, 50 μm.

longer exists in clone 4.1 cells with persistent tau aggregates, implying cellular adaptation to the long-term presence of tau aggregates.

Differential Responses of UPS to Tau and α-Syn Aggregates—Earlier studies from our lab demonstrated that Lewy body-like α-Syn aggregates induced by transduction of α-Syn PFFs interact not only with autophagy machinery but also with the UPS components, although neither system is able to degrade the aggregates (24, 29). Surprisingly, both nascent tau inclusions in newly transduced clone 4 cells and long-term propagated tau inclusions in clone 4.1 cells rarely showed colocalization with ubiquitin or the 20S proteasome subunit (the catalytic core of

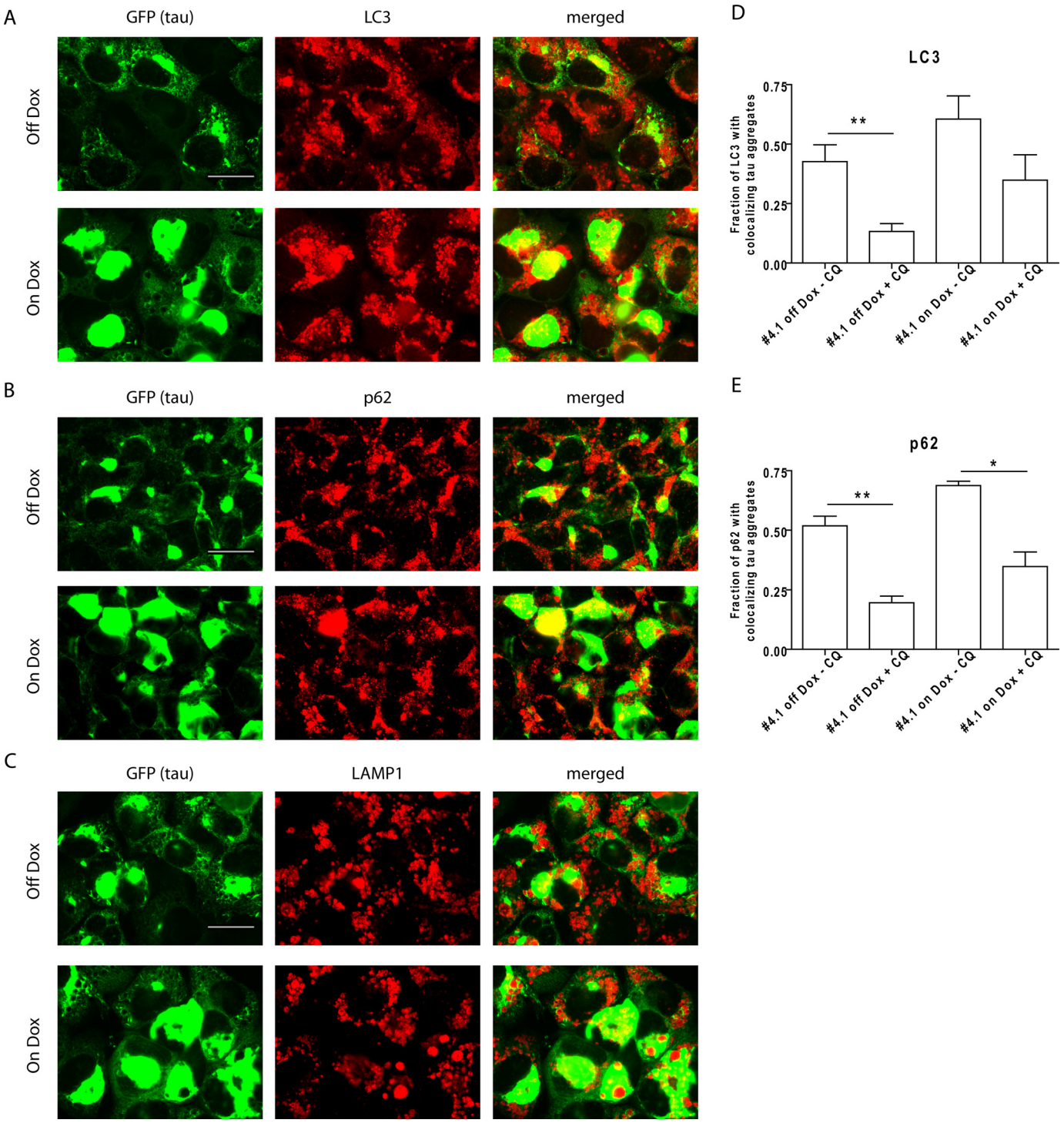

FIGURE 8. **Reduced colocalization between tau aggregates and autophagy markers with lysosomal inhibition.** *A–C*, immunostaining of LC3, p62, and LAMP1 for CQ-treated clone 4.1 cells that were either removed from Dox for 4–5 days (*Off Dox*) or maintained on Dox (*On Dox*). Tau aggregates were visualized by GFP signals. Cells were treated with 30 μM CQ for 1 day before fixing. *Scale bars*, 50 μm. *D* and *E*, Manders coefficient measuring the fraction of LC3 or p62 signals with overlapping tau aggregates for clone 4.1 cells with and without CQ treatment. Quantification was based on 3 independent sets of experiments. Data are shown as mean ± S.E. Within *off Dox* or *on Dox* groups, Student's *t* test was performed for comparisons between cells with and without a 1-day CQ treatment. *, $p < 0.05$. **, $p < 0.005$.

proteasome) when soluble proteins were extracted during fixing (Fig. 10, *A* and *B*, for newly transduced clone 4; data not shown for clone 4.1), although the extent of colocalization with ubiquitin was significantly higher in the newly transduced clone 4 cells based on Manders coefficients (Fig. 10*E*). Consistent with our previous studies, α-Syn aggregates induced in clone 4.1 cells by transient transfection of α-Syn and transduction of α-syn PFFs were extensively colocalized with ubiquitin and 20S immunoreactivities (Fig. 10, *C* and *D*), with Manders coefficient for the fraction area of α-Syn aggregates overlapping with ubiquitin or 20S immunoreactivities overwhelmingly higher than that for tau aggregates in

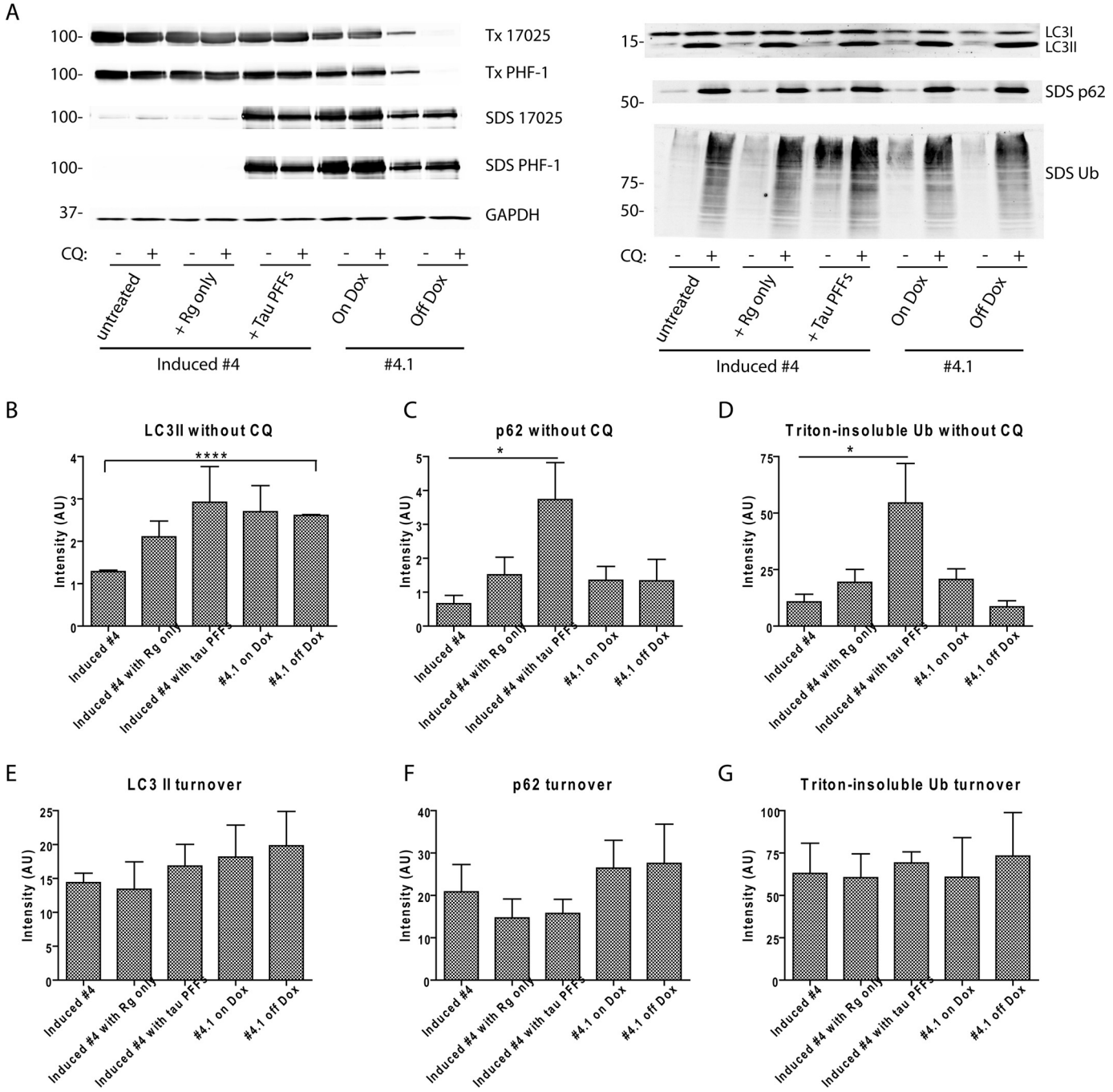

FIGURE 9. **Tau aggregation does not lead to significant impairment of autophagy flux.** *A*, autophagy flux assay was conducted on 5 groups of cells: 1) induced clone 4 cells, 2) induced clone 4 cells newly treated with BioPORTER reagent, 3) induced clone 4 cells newly transduced with tau PFFs mediated by BioPORTER reagent, 4) clone 4.1 cells maintained on Dox, and 5) clone 4.1 cells withdrawn from Dox for 5 days. Levels of autophagy substrates (LC3-II, p62, and Triton (*Tx*)-insoluble ubiquitinated proteins) were compared for each group of cells with and without 2 days treatment of 30 μM CQ that blocked lysosomal degradation. Although LC3-II was completely extracted by 1% Triton X-100 lysis buffer, p62 was predominantly found in the SDS fraction. Differential solubility of tau in these 5 groups of cells was confirmed by immunoblotting with 17025 and PHF-1. GAPDH served as loading control. Immunoblots from one representative set of experiment were shown. *B–D*, densitometry quantification of LC3-II, p62, and Triton-insoluble ubiquitinated proteins for the experimental conditions shown. *E–G*, turnover of the three types of autophagy substrates during the 2-day period was estimated by (level with CQ treatment − level without CQ treatment). For *B–G*, quantification was based on 4 independent sets of experiment, except for $n = 3$ for clone 4.1 cells off Dox. Data are shown as mean ± S.E. *, $p < 0.05$. ****, $p < 0.0000005$.

newly transduced clone 4 cells (Fig. 10, *E* and *F*), although both types of protein aggregates were newly formed under the respective experimental paradigms. Meanwhile, increased colocalization with ubiquitin and the 20S subunit were observed for persistent tau aggregates in clone 4.1 cells when α-Syn aggregates were induced in the same cells (Fig. 10, *E* and *F*), probably because of frequent association between the two kinds of aggregates (Fig. 10, *C* and *D*). These results suggest the UPS is not indiscriminately activated by the formation of any protein aggregates, whereby strong responses are mounted toward α-Syn aggregates, whereas tau aggregates are largely ignored in our cellular system.

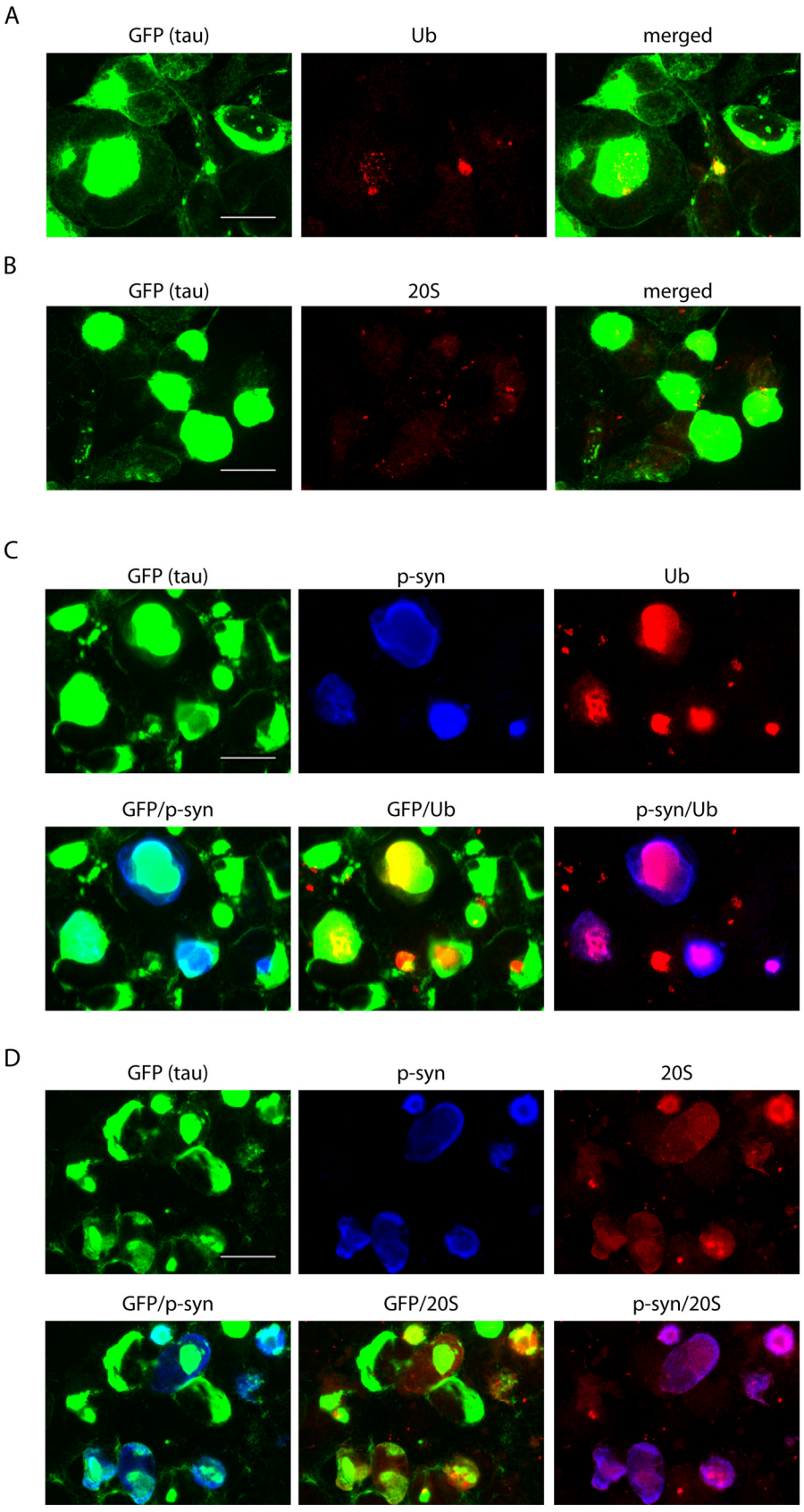
A
GFP (tau)
Ub
merged
B
GFP (tau)
20S
merged
C
GFP (tau)
p-syn
Ub
GFP/p-syn
GFP/Ub
p-syn/Ub
D
GFP (tau)
p-syn
20S
GFP/p-syn
GFP/20S
p-syn/20S

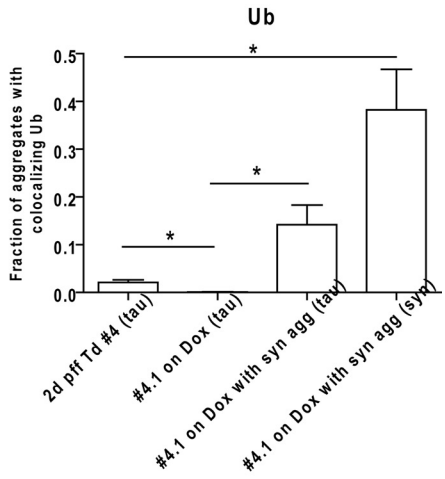
E
Ub
Fraction of aggregates with colocalizing Ub
0.5
0.4
0.3
0.2
0.1
0.0
*
*
*
2d pff Td #4 (tau)
#4.1 on Dox (tau)
#4.1 on Dox with syn agg (tau)
#4.1 on Dox with syn agg (syn)

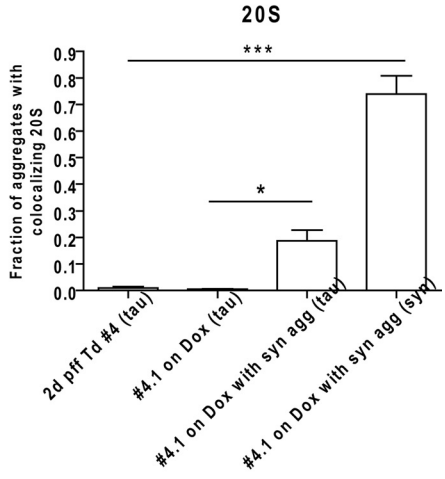
F
20S
Fraction of aggregates with colocalizing 20S
0.9
0.8
0.7
0.6
0.5
0.4
0.3
0.2
0.1
0.0
***
*
2d pff Td #4 (tau)
#4.1 on Dox (tau)
#4.1 on Dox with syn agg (tau)
#4.1 on Dox with syn agg (syn)

Interestingly, although both neurofibrillary tangles and Lewy bodies are partially ubiquitinated in the diseased brains, neuropathological studies reported far more extensive associations of proteasomes with Lewy bodies than with neurofibrillary tangles (30, 31).

Discussion

By using a cell line with inducible expression of tau, we demonstrated that even high burdens of tau aggregates can be gradually removed with extended suppression of soluble tau expression, and the ALP is at least partially mediating the clearance process. Nevertheless, a small amount of aggregates remaining at the end of the clearance phase can lead to rapid re-emergence of robust tau pathology once soluble tau expression is restored. In addition, live imaging of these aggregate-bearing cells revealed that tau aggregates are dynamic structures that can undergo fusion and fission, and they can be stably carried in dividing cells due to ready partitioning into daughter cells during mitosis.

In the past few years, mounting evidence suggests that protein aggregates involved in various neurodegenerative diseases, including tau aggregates, are self-amplifying entities that can propagate along neuroanatomical connections, leading to disease progression from restricted brain areas in the early phase of the disease to widespread brain regions in the later stages (reviewed by Ref. 32). *In vitro* studies on disease-associated proteins such as prion and tau showed that fragmentation of long fibrils, usually achieved by sonication, is critical for efficient seeded amplification (33, 34). Moreover, it has been further demonstrated that only short tau fibrils, but not long fibrils, can be internalized and transported by neurons (35). Therefore, it is unclear how the bulky, apparently immobile tau inclusions detected in the tauopathy brains could undergo cell-to-cell transmission. Previous studies suggested that molecules within fibrillar aggregates can freely dissociate from one filament and re-associate with another filament (36, 37). This dynamic equilibrium between aggregates and their subunits was also supported by an *in vivo* study on tau (38). By visualizing GFP-tagged tau aggregates in living cells, our current study provides direct evidence of the dynamics of intracellular tau aggregates at the macroscopic level. Not surprisingly, small tau aggregates appear to be mobile entities that are highly diffusible in cells and have a great propensity to coalesce into larger aggregates when soluble tau expression is high. More interestingly, even visually cumbersome aggregates can readily undergo morphological restructuring and fracture into smaller pieces during cell division, which get passed along into daughter cells. In some instances, small aggregates also seemed to dissociate from the edge of large aggregates in the absence of cell division. Assuming that this dynamic nature of tau aggregates also occurs in neurons, these results suggest that seemingly inert tau inclusions can release small seeds for transport along axons, with subsequent release and spreading to other neurons. Furthermore, fragmentation of tau aggregates into daughter cells offers a potential mechanistic explanation for pathological tau transmission in glial cells, which are shown to proliferate in neurodegenerative diseases (reviewed by Ref. 39).

We showed here that the ALP was involved in the clearance of tau aggregates when soluble tau expression was turned off, as supported by frequent colocalization of focal tau inclusions with autophagy markers and slower reduction of insoluble tau upon lysosomal inhibition. However, it is possible that spontaneous disassembly of tau aggregates into smaller species, such as oligomers and even monomers, may also be taking place. In fact, it has been demonstrated *in vitro* that amyloid fibrils made up of tau, Aβ, or α-Syn readily undergo disaggregation when diluted in monomer-free solution (27, 40–42), which is somewhat analogous to the cellular condition when soluble tau expression is suppressed. Reduced concentration of soluble tau in the cytoplasm may shift the dynamic equilibrium of tau aggregation, resulting in a net disassembly of aggregates. This hypothesis of concentration-dependent equilibrium is supported by live imaging of clone 4.1 cells, which showed that dissociation of small aggregates from large inclusions was accompanied by a gradual decrease in the overall sizes of aggregates when tau expression was turned off, but not when cells were highly expressing tau. Moreover, ineffective lysosomal degradation of insoluble tau when tau expression is high in our cell model suggests the ALP may be incapable of handling relatively bulky tau aggregates, although the latter appear to be actively recruiting autophagosomes. Therefore, spontaneous disintegration of large tau aggregates is likely occurring upon suppression of tau expression to facilitate degradation by the ALP. The lack of obvious colocalization of lysosomes with tau inclusions may imply that the conspicuous aggregates are rarely delivered into the lysosomes, and that the actual tau species being degraded are probably very short filaments or oligomers that dissociate from the large aggregates during disassembly.

Although prior work (12) and our study suggest it is possible to remove intracellular tau aggregates by suppressing soluble tau expression, there are several factors that should be considered in adopting this strategy as a therapeutic approach for tauopathies. First, one of the detrimental consequences of tau aggregation is suggested to be reduced microtubule stability due to sequestration of soluble tau (43). This deficit will be exacerbated by reducing tau expression. Second, our study reveals that even miniscule amounts of tau aggregates remaining after clearance are sufficient to promote robust pathology if soluble tau expression is restored, and irreversible clearance

FIGURE 10. **Differential interactions of UPS with tau and α-syn aggregates.** *A* and *B*, ubiquitin and 20S staining for induced clone 4 cells at 2 days after tau PFF transduction. *C* and *D*, ubiquitin and 20S staining for clone 4.1 cells with transiently induced α-syn aggregates at 1 or 2 days after α-syn PFF transduction. Tau aggregates were visualized by GFP signals. α-Syn aggregates were labeled by antibodies specific for phosphorylated α-Syn (*p-syn*). Soluble proteins were extracted by 1% Triton X-100 during fixing. *Scale bars*, 50 μm. *E* and *F*, Manders coefficient for the fraction of area occupied by tau or α-Syn aggregates with colocalizing ubiquitin or 20S signals. Four conditions were quantified: 1) tau aggregates in clone 4 cells at 2 days after tau PFF transduction, 2) tau aggregates in clone 4.1 cells, 3) tau aggregates in clone 4.1 cells with transiently induced α-syn aggregates, and 4) transiently induced α-Syn aggregates in clone 4.1 cells. Quantification was based on 3 independent sets of experiments. Data are shown as mean ± S.E. The following pairwise comparisons were made using Student's *t* test: 1 *versus* 2, 2 *versus* 3, and 1 *versus* 4. *, $p < 0.05$. ***, $p < 0.0005$.

only occurred with a more extended period of soluble tau removal. Moreover, in an earlier study using transgenic mice with inducible expression of tau, neurofibrillary tangles continued to accumulate in mice when the suppression of soluble tau expression was incomplete (8). These findings pose challenges for a potential therapeutic approach of reducing normal tau, as it is unclear how long it would take for well established tau inclusions to be thoroughly cleared from human brains without residual seeding-competent tau species, and it is also technically challenging and potentially unsafe to maintain appreciable suppression of tau expression on a long-term basis. Third, our live imaging experiment showed that small tau aggregates generated during the clearance phase are exceptionally mobile, rendering them possibly even more harmful to cells than the bulkier and more consolidated aggregates, as has been proposed for oligomers and protofibrils (reviewed in Refs. 44 and 45). Moreover, the highly diffusible misfolded tau seeds, if not thoroughly cleared, may spread more readily along neuroanatomically connected pathways, leading to even wider distribution of pathology once tau expression is resumed.

Our observation that QBI-293 cells are able to stably propagate tau inclusions for months without obvious cellular toxicity suggests aggregated tau could be well tolerated by cells. Although we cannot exclude intrinsic differences in resilience between immortalized dividing cells in culture and post-mitotic neurons in human brain, our study reveals that the toxicity of tau aggregates could be partly determined by their effects on protein degradation systems. In our clone 4.1 cells, despite local recruitment of autophagosomes by tau aggregates, there is no appreciable accumulation of ALP components overall and the autophagy flux remains normal. We also found few interactions between the UPS and tau inclusions. In short, both the UPS and ALP are not strongly responding to tau aggregation and remain largely unperturbed in our cell model. On the other hand, significant accumulation of autophagic vacuoles (pre-lysosomal autophagy vesicles) is observed in AD brains, especially in the dystrophic neurites and perikarya of neurons containing tau filaments (46). Also unlike our cell model, a subset of neurofibrillary tangles are ubiquitinated in AD brains, although ubiquitination was suggested to be a late event (47–49). Because degradation by UPS requires unfolding and translocation of substrates into the catalytic core of proteasome, this pathway is ill-suited at degrading physically cumbersome protein aggregates. Our current study suggests that, despite a modulatory role of the ALP in clearing tau aggregates when soluble tau expression is suppressed, the ALP is also inefficient at handling large tau aggregates, and similar findings were made in our earlier study on α-Syn aggregates (24). Furthermore, when cells fail to clear large tau or α-Syn aggregates by activating both UPS and ALP, the excessive engagement of degradation machineries with aggregates may actually compromise the degradation of other proteins, resulting in cellular dysfunction in the long run. In fact, reduced proteasome activity found in AD brains was demonstrated to be caused by neurofibrillary tangles interacting with proteasomes (50, 51). Therefore, whereas it is generally believed that activating cellular degradation systems represents a promising therapeutic strategy for neurodegenerative diseases characterized by protein aggregation, our studies lead us to propose that a more beneficial approach may be to identify means to inhibit unproductive interactions between protein aggregates and components of the protein degradation systems, so as to free the latter for their normal functions.

In conclusion, our data provide new understandings of the dynamics of tau aggregates in mediating cell-to-cell transmission in dividing cells and perhaps in neurons. Moreover, our elucidation of the turnover of tau aggregates, as well as their interactions with protein degradation systems, offers new insights into potential therapeutic strategies for neurodegenerative tauopathies. In particular, our data raise concerns about a therapeutic approach of lowering tau expression, and call for a reconsideration of therapeutic attempts to enhance protein degradation systems. Indeed, our results suggest that small molecules or biologics that can prevent tau aggregates from engaging cellular degradation machineries may allow for the continued function of these critical cellular components, thereby reducing cellular stress and toxicity.

Author Contributions—J. L. G. conceived and designed the study, performed and analyzed the experiments, and wrote the paper. V. M. L., D. M., and K. R. B. conceived, designed and coordinated the study, and edited the paper. A. B., A. S., K. C., S. C., F. S., J. P. D., B. E. Z., and A. C. performed and analyzed the experiments. All authors reviewed the results and approved the final version of the manuscript.

Acknowledgments—We thank Dawn Riddle, Lakshmi Changolkar, and Chris Chung for technical assistance, Dr. Selcuk Tanik for technical advice, and all the other members of the Center for Neurodegenerative Disease Research for their help and support. Monoclonal antibody PHF-1 was a generous gift from Dr. Peter Davies.

References

1. Lee, V. M., Goedert, M., and Trojanowski, J. Q. (2001) Neurodegenerative tauopathies. *Annu. Rev. Neurosci.* **24,** 1121–1159
2. Cleveland, D. W., Hwo, S. Y., and Kirschner, M. W. (1977) Purification of tau, a microtubule-associated protein that induces assembly of microtubules from purified tubulin. *J. Mol. Biol.* **116,** 207–225
3. Drechsel, D. N., Hyman, A. A., Cobb, M. H., and Kirschner, M. W. (1992) Modulation of the dynamic instability of tubulin assembly by the microtubule-associated protein tau. *Mol. Biol. Cell* **3,** 1141–1154
4. Ballatore, C., Lee, V. M., and Trojanowski, J. Q. (2007) tau-mediated neurodegeneration in Alzheimer's disease and related disorders. *Nat. Rev. Neurosci.* **8,** 663–672
5. Arriagada, P. V., Growdon, J. H., Hedley-Whyte, E. T., and Hyman, B. T. (1992) Neurofibrillary tangles but not senile plaques parallel duration and severity of Alzheimer's disease. *Neurology* **42,** 631–639
6. Ling, H., Ling, H., de Silva, R., Massey, L. A., Courtney, R., Hondhamuni, G., Bajaj, N., Lowe, J., Holton, J. L., Lees, A., and Revesz, T. (2014) Characteristics of progressive supranuclear palsy presenting with corticobasal syndrome: a cortical variant. *Neuropathol. Appl. Neurobiol.* **40,** 149–163
7. Kouri, N., Murray, M. E., Hassan, A., Rademakers, R., Uitti, R. J., Boeve, B. F., Graff-Radford, N. R., Wszolek, Z. K., Litvan, I., Josephs, K. A., and Dickson, D. W. (2011) Neuropathological features of corticobasal degeneration presenting as corticobasal syndrome or Richardson syndrome. *Brain* **134,** 3264–3275
8. Santacruz, K., Lewis, J., Spires, T., Paulson, J., Kotilinek, L., Ingelsson, M., Guimaraes, A., DeTure, M., Ramsden, M., McGowan, E., Forster, C., Yue, M., Orne, J., Janus, C., Mariash, A., Kuskowski, M., Hyman, B., Hutton, M., and Ashe, K. H. (2005) Tau suppression in a neurodegenerative mouse model improves memory function. *Science* **309,** 476–481

9. Wittmann, C. W., Wszolek, M. F., Shulman, J. M., Salvaterra, P. M., Lewis, J., Hutton, M., and Feany, M. B. (2001) Tauopathy in *Drosophila*: neurodegeneration without neurofibrillary tangles. *Science* **293,** 711–714
10. Yoshiyama, Y., Higuchi, M., Zhang, B., Huang, S. M., Iwata, N., Saido, T. C., Maeda, J., Suhara, T., Trojanowski, J. Q., and Lee, V. M. (2007) Synapse loss and microglial activation precede tangles in a P301S tauopathy mouse model. *Neuron* **53,** 337–351
11. Weingarten, M. D., Lockwood, A. H., Hwo, S. Y., and Kirschner, M. W. (1975) A protein factor essential for microtubule assembly. *Proc. Natl. Acad. Sci. U.S.A.* **72,** 1858–1862
12. Polydoro, M., de Calignon, A., Suárez-Calvet, M., Sanchez, L., Kay, K. R., Nicholls, S. B., Roe, A. D., Pitstick, R., Carlson, G. A., Gómez-Isla, T., Spires-Jones, T. L., and Hyman, B. T. (2013) Reversal of neurofibrillary tangles and tau-associated phenotype in the rTgTauEC model of early Alzheimer's disease. *J. Neurosci.* **33,** 13300–13311
13. Rubinsztein, D. C. (2006) The roles of intracellular protein-degradation pathways in neurodegeneration. *Nature* **443,** 780–786
14. Chesser, A. S., Pritchard, S. M., and Johnson, G. V. (2013) Tau clearance mechanisms and their possible role in the pathogenesis of Alzheimer disease. *Front. Neurol.* **4,** 122
15. Krüger, U., Wang, Y., Kumar, S., and Mandelkow, E. M. (2012) Autophagic degradation of tau in primary neurons and its enhancement by trehalose. *Neurobiol. Aging* **33,** 2291–2305
16. Schaeffer, V., Lavenir, I., Ozcelik, S., Tolnay, M., Winkler, D. T., and Goedert, M. (2012) Stimulation of autophagy reduces neurodegeneration in a mouse model of human tauopathy. *Brain* **135,** 2169–2177
17. Caccamo, A., Magrì, A., Medina, D. X., Wisely, E. V., Lopez-Aranda, M. F., Silva, A. J., and Oddo, S. (2013) mTOR regulates tau phosphorylation and degradation: implications for Alzheimer's disease and other tauopathies. *Aging Cell* **12,** 370–380
18. Guo, J. L., and Lee, V. M. (2011) Seeding of normal Tau by pathological tau conformers drives pathogenesis of Alzheimer-like tangles. *J. Biol. Chem.* **286,** 15317–15331
19. Iba, M., Guo, J. L., McBride, J. D., Zhang, B., Trojanowski, J. Q., and Lee, V. M. (2013) Synthetic Tau fibrils mediate transmission of neurofibrillary tangles in a transgenic mouse model of Alzheimer's-like tauopathy. *J. Neurosci.* **33,** 1024–1037
20. Bi, X., Haque, T. S., Zhou, J., Skillman, A. G., Lin, B., Lee, C. E., Kuntz, I. D., Ellman, J. A., and Lynch, G. (2000) Novel cathepsin D inhibitors block the formation of hyperphosphorylated tau fragments in hippocampus. *J. Neurochem.* **74,** 1469–1477
21. Hamano, T., Gendron, T. F., Causevic, E., Yen, S. H., Lin, W. L., Isidoro, C., Deture, M., and Ko, L. W. (2008) Autophagic-lysosomal perturbation enhances tau aggregation in transfectants with induced wild-type tau expression. *Eur. J. Neurosci.* **27,** 1119–1130
22. Inoue, K., Rispoli, J., Kaphzan, H., Klann, E., Chen, E. I., Kim, J., Komatsu, M., and Abeliovich, A. (2012) Macroautophagy deficiency mediates age-dependent neurodegeneration through a phospho-tau pathway. *Mol. Neurodegen.* **7,** 48
23. Li, W., and Lee, V. M. (2006) Characterization of two VQIXXK motifs for tau fibrillization *in vitro*. *Biochemistry* **45,** 15692–15701
24. Tanik, S. A., Schultheiss, C. E., Volpicelli-Daley, L. A., Brunden, K. R., and Lee, V. M. (2013) Lewy body-like α-synuclein aggregates resist degradation and impair macroautophagy. *J. Biol. Chem.* **288,** 15194–15210
25. Rubinsztein, D. C., Cuervo, A. M., Ravikumar, B., Sarkar, S., Korolchuk, V., Kaushik, S., and Klionsky, D. J. (2009) In search of an "autophagomometer." *Autophagy* **5,** 585–589
26. Ravikumar, B., Sarkar, S., Davies, J. E., Futter, M., Garcia-Arencibia, M., Green-Thompson, Z. W., Jimenez-Sanchez, M., Korolchuk, V. I., Lichtenberg, M., Luo, S., Massey, D. C., Menzies, F. M., Moreau, K., Narayanan, U., *et al.* (2010) Regulation of mammalian autophagy in physiology and pathophysiology. *Physiol. Rev.* **90,** 1383–1435
27. Shammas, S. L., Garcia, G. A., Kumar, S., Kjaergaard, M., Horrocks, M. H., Shivji, N., Mandelkow, E., Knowles, T. P., Mandelkow, E., and Klenerman, D. (2015) A mechanistic model of tau amyloid aggregation based on direct observation of oligomers. *Nat. Commun.* **6,** 7025
28. Mizushima, N., Yoshimori, T., and Levine, B. (2010) Methods in mammalian autophagy research. *Cell* **140,** 313–326
29. Luk, K. C., Song, C., O'Brien, P., Stieber, A., Branch, J. R., Brunden, K. R., Trojanowski, J. Q., and Lee, V. M. (2009) Exogenous α-synuclein fibrils seed the formation of Lewy body-like intracellular inclusions in cultured cells. *Proc. Natl. Acad. Sci. U.S.A.* **106,** 20051–20056
30. Kwak, S., Masaki, T., Ishiura, S., and Sugita, H. (1991) Multicatalytic proteinase is present in Lewy bodies and neurofibrillary tangles in diffuse Lewy body disease brains. *Neurosci. Lett.* **128,** 21–24
31. Ii, K., Ito, H., Tanaka, K., and Hirano, A. (1997) Immunocytochemical co-localization of the proteasome in ubiquitinated structures in neurodegenerative diseases and the elderly. *J. Neuropathol. Exp. Neurol.* **56,** 125–131
32. Guo, J. L., and Lee, V. M. (2014) Cell-to-cell transmission of pathogenic proteins in neurodegenerative diseases. *Nat. Med.* **20,** 130–138
33. Meyer, V., Dinkel, P. D., Rickman Hager, E., and Margittai, M. (2014) Amplification of tau fibrils from minute quantities of seeds. *Biochemistry* **53,** 5804–5809
34. Knowles, T. P., Waudby, C. A., Devlin, G. L., Cohen, S. I., Aguzzi, A., Vendruscolo, M., Terentjev, E. M., Welland, M. E., and Dobson, C. M. (2009) An analytical solution to the kinetics of breakable filament assembly. *Science* **326,** 1533–1537
35. Wu, J. W., Herman, M., Liu, L., Simoes, S., Acker, C. M., Figueroa, H., Steinberg, J. I., Margittai, M., Kayed, R., Zurzolo, C., Di Paolo, G., and Duff, K. E. (2013) Small misfolded tau species are internalized via bulk endocytosis and anterogradely and retrogradely transported in neurons. *J. Biol. Chem.* **288,** 1856–1870
36. Carulla, N., Caddy, G. L., Hall, D. R., Zurdo, J., Gairí, M., Feliz, M., Giralt, E., Robinson, C. V., and Dobson, C. M. (2005) Molecular recycling within amyloid fibrils. *Nature* **436,** 554–558
37. Belitzky, A., Melamed-Book, N., Weiss, A., and Raviv, U. (2011) The dynamic nature of amyloid β(1–40) aggregation. *Phys. Chem. Chem. Phys.* **13,** 13809–13814
38. Sydow, A., and Mandelkow, E. M. (2010) 'Prion-like' propagation of mouse and human tau aggregates in an inducible mouse model of tauopathy. *Neurodegener. Dis.* **7,** 28–31
39. Glass, C. K., Saijo, K., Winner, B., Marchetto, M. C., and Gage, F. H. (2010) Mechanisms underlying inflammation in neurodegeneration. *Cell* **140,** 918–934
40. Harper, J. D., Wong, S. S., Lieber, C. M., and Lansbury, P. T., Jr. (1999) Assembly of A beta amyloid protofibrils: an *in vitro* model for a possible early event in Alzheimer's disease. *Biochemistry* **38,** 8972–8980
41. Cremades, N., Cohen, S. I., Deas, E., Abramov, A. Y., Chen, A. Y., Orte, A., Sandal, M., Clarke, R. W., Dunne, P., Aprile, F. A., Bertoncini, C. W., Wood, N. W., Knowles, T. P., Dobson, C. M., and Klenerman, D. (2012) Direct observation of the interconversion of normal and toxic forms of α-synuclein. *Cell* **149,** 1048–1059
42. Tang, L., Li, H. T., Du, H. N., Zhang, F., Hu, X. F., and Hu, H. Y. (2006) Study of the disassembly-assembly process of α-synuclein fibrils by in situ atomic force microscopy. *Micron* **37,** 675–679
43. Brunden, K. R., Zhang, B., Carroll, J., Yao, Y., Potuzak, J. S., Hogan, A. M., Iba, M., James, M. J., Xie, S. X., Ballatore, C., Smith, A. B., 3rd, Lee, V. M., and Trojanowski, J. Q. (2010) Epothilone D improves microtubule density, axonal integrity, and cognition in a transgenic mouse model of tauopathy. *J. Neurosci.* **30,** 13861–13866
44. Caughey, B., and Lansbury, P. T. (2003) Protofibrils, pores, fibrils, and neurodegeneration: separating the responsible protein aggregates from the innocent bystanders. *Annu. Rev. Neurosci.* **26,** 267–298
45. Haass, C., and Selkoe, D. J. (2007) Soluble protein oligomers in neurodegeneration: lessons from the Alzheimer's amyloid beta-peptide. *Nat. Rev. Mol. Cell Biol.* **8,** 101–112
46. Nixon, R. A., Wegiel, J., Kumar, A., Yu, W. H., Peterhoff, C., Cataldo, A., and Cuervo, A. M. (2005) Extensive involvement of autophagy in Alzheimer disease: an immuno-electron microscopy study. *J. Neuropathol. Exp. Neurol.* **64,** 113–122
47. Cole, G. M., and Timiras, P. S. (1987) Ubiquitin-protein conjugates in Alzheimer's lesions. *Neurosci. Lett.* **79,** 207–212
48. Brion, J. P., Power, D., Hue, D., Couck, A. M., Anderton, B. H., and Flament-Durand, J. (1989) Heterogeneity of ubiquitin immunoreactivity in neurofibrillary tangles of Alzheimer's disease. *Neurochem. Int.* **14,** 121–128

49. He, Y., Duyckaerts, C., Delaère, P., Piette, F., and Hauw, J. J. (1993) Alzheimer's lesions labelled by anti-ubiquitin antibodies: comparison with other staining techniques: a study of 15 cases with graded intellectual status in ageing and Alzheimer's disease. *Neuropathol. Appl. Neurobiol.* **19,** 364–371
50. Keck, S., Nitsch, R., Grune, T., and Ullrich, O. (2003) Proteasome inhibition by paired helical filament-tau in brains of patients with Alzheimer's disease. *J. Neurochem.* **85,** 115–122
51. Keller, J. N., Hanni, K. B., and Markesbery, W. R. (2000) Impaired proteasome function in Alzheimer's disease. *J. Neurochem.* **75,** 436–439
52. Ishihara, T., Hong, M., Zhang, B., Nakagawa, Y., Lee, M. K., Trojanowski, J. Q., and Lee, V. M. (1999) Age-dependent emergence and progression of a tauopathy in transgenic mice overexpressing the shortest human tau isoform. *Neuron* **24,** 751–762
53. Sampathu, D. M., Neumann, M., Kwong, L. K., Chou, T. T., Micsenyi, M., Truax, A., Bruce, J., Grossman, M., Trojanowski, J. Q., and Lee, V. M. (2006) Pathological heterogeneity of frontotemporal lobar degeneration with ubiquitin-positive inclusions delineated by ubiquitin immunohistochemistry and novel monoclonal antibodies. *Am. J. Pathol.* **169,** 1343–1352
54. Waxman, E. A., and Giasson, B. I. (2008) Specificity and regulation of casein kinase-mediated phosphorylation of α-synuclein. *J. Neuropathol. Exp. Neurol.* **67,** 402–416